Article:

Zhu, F and Heitor, A orcid.org/0000-0002-2346-8250 (2022) Influence of Water Content on Track Degradation at Transition Zones. Transportation Infrastructure Geotechnology, 9 (1). pp. 32-53. ISSN 2196-7202

https://doi.org/10.1007/s40515-021-00151-0

Influence of water content on track degradation at transition zones

Fangda Zhu BEng, MSc (corresponding author)
School of Civil Engineering, University of Leeds, Leeds, UK
ml18f4z@leeds.ac.uk

Ana Heitor LicEng, MEng, PhD, MIEAust
Lecturer in Geotechnical Engineering, School of Civil Engineering, University of Leeds, Leeds, UK
a.heitor@leeds.ac.uk

Submitted to: **Transportation Infrastructure Geotechnology**

Words: 8750 (excluding abstract and references)

Figures: 21

Tables: 9

ABSTRACT

This study aims to explore the role of water retention behaviour in the track degradation of the transition zone by examining the influence of water content variation. A model of railway bridge approach transition was built in the PLAXIS 3D to simulate the track degradation under diverse water content scenarios. A wedge-shaped backfill with unbound granular material (UGM) was simulated as a technical solution between the bridge abutment and open track. The most distinctive characteristic of the model is that the direct relationship between soil water content and soil displacement can be explored. To achieve this, the seasonal change in the soil moisture content of subsoil was simulated as the independent variable. The water content variation adopted mimicked the wet season (ω= 7.6%), as-compacted (ω= 5.6%) and dry season (ω= 3.6%) water content conditions. The results indicate that higher soil strains and displacements are obtained for high water contents. This indicates that there is a clear correlation between soil water retention and track displacements. In addition, the results suggest that a reduction in water content in the track substructure can be effective in mitigating in service settlement as overall track stiffness increases as a result. However, this effect is more pronounced at the track level and becomes less importance at higher depth in the formation layer. This study also shows that the bump from the bridge structure to backfill can be mitigated and smooth track geometry from the backfill and the open track can be achieved by manipulating the water content.

Keywords: Transition zones, Transition wedge, water content

1 Introduction

Track degradation is a major problem in the railway transitions (or approaches), and the main cause of frequent track maintenance works. Compared with the other sections in the railway, the transition zone between the abutment and embankments is an area requiring frequent inspection and high maintenance costs due to the geometric failure. Figure 1 shows a settlement comparison between the different sections of track, i.e. on the bridge, approach and open track (Li and Davis, 2005). It can be observed that larger settlements occur in the approach and exceeds that of open track despite having a higher stiffness. These excessive settlements lead to the deterioration of track geometry and thus require frequent and costly repair maintenance. For instance, the maintenance requirements in the transition zones can be up to eight times higher than the normal section of track (Varandas et al., 2014), and can amount to 110 million dollars and 200 million dollars annually in Europe and USA, respectively (Sañudo et al., 2016). Past studies have shown that larger incidence of track settlement in these locations are mainly due to difference in stiffness between a relatively rigid approach to a relatively soft open track supported for subsoil formations.

This paper explores the role of water retention in the degradation of the railway transition. The factors related to hydraulic condition change are vital contributors to differential settlement and seriously affect the track performance. The excessive settlement in substructure can be mitigated by simulating the in-situ scenarios and exploring the optimum value of the moisture content of compacted soil. A direct relationship between water content and degradation has yet to be adequately defined. To explore the relationship between soil strain and its water retention behaviour, the numerical analysis is required. This paper presents a numerical analysis based on the PLAXIS 3D a finite element software.

2. Railway transitions

Transitions may be defined as locations where there is a change in railway track stiffness from ballasted track to a fixed track structure, such as concrete slab-track or a fixed bridge deck. They can be classified in different categories, i.e. abutment to embankment transition, ballast track to slab track transition, bridge to embankment transition (Woodward et al., 2014), at the tunnel entrance and exits, at railway grade crossings, at locations where rigid culverts are installed in ballasted track (Kerr and Moroney, 1995) (Gallego et al., 2012).

Failures and performance shortcomings in a bridge approach transition zone, can arise from a range of different factors and those are summarized in Figure 2 (Gallage et al., 2013a). Among those, one of the most typical structural problems is degradation that can lead to several problems regarding the rail geometry, vehicle movement and passenger ride quality. While the track degradation of the transition zone is mainly caused by the change in vertical stiffness, other factors also play a role, i.e. settlement in ballast, subballast derived from fouling, fill and subgrade deformation, and the track damping characteristics (Mishra et al., 2014). In addition, under repeated loads, a high degree of plastic strain will be accumulated in the ballast layer under high speed railway, because of the densification or particle breakdown under high and intense vertical and lateral force (Kennedy et al., 2013). Gallage et al. (2013b) postulated that there are three mechanisms causing the degradation in the transition. They are subgrade attrition, massive subgrade shear failure, and excessive consolidation settlement. The degradation might be catalysed by the reduction in shear strength of subgrade soil due to the change in water content (Gallage et al., 2013b).

2.3 Resilient modulus and the role of water content

Past studies recognise the critical role played by the soil moisture content and its influence on the resilient modulus and stiffness (Liang et al., 2008). While there have been several correlations between soil resilient modulus and moisture content proposed, there is a general agreement that the resilient modulus increases with decreasing moisture content. Seed et al. (1962) proposed a correlation illustrated in Figure 3, which resulted by the 27 repeated load triaxial tests on the railway subgrade fine-grained soil and plotted as the theory of. In Figure 3, the M / M_{opt} denotes the ratio between the resilient modulus at a given water content to the resilient modulus at optimum water content. The negative correlation can be clearly observed, which was also found by the literature (Sauer and Monismith, 1968) (Culley, 1971) (Robnett and Thompson, 1976) (Fredlund et al., 1977) (Edil and Motan, 1979) (Elfino and Davidson, 1989).

Figure 4 illustrates the resilient modulus of subgrade soils under repeated traffic loading (Huang, 1993). The resilient modulus indicates the soil stiffness or stress-strain relationship under the repeated loads or traffic loads (Kodikara and Yeo, 2015). For instance, Seed et al. proposed that the resilient modulus is influenced by only bulk stress (Seed et al., 1967), however, tests done on the subgrade soil indicated that the magnitude of deviator stress has a greater effect than the confining pressure (Li and Selig, 1994). However, soil properties and some external parameters also affect the resilience modulus. A systematic study on the dependency of resilient modulus on compaction method and relative compaction, moisture content and its seasonal change, soil mineral properties and its plastic index has been conducted by (Dhir et al., 2019). The railway subgrade always undergoes some risks from water variation during service, such as infiltration resulting from precipitation and evaporation, inundation and overtopping, flooding and rising level of the water table (Yang et al., 2005). The resilient modulus is found to be sensitive to the periodic change in water content (Liang et al., 2008). The resilient modulus for fine-grained soil in subgrade was determined by the **Equation 1** proposed by Drumm, E. C., and R. Meier (Drumm and Meier, 2003) and based on the climatic model from *MEPDG* (Olidid and Hein, 2004). Drumm, E.C. and R.Meier created the linear relationship between volumetric water content and the resilient modulus, but it did not include any parameter related to stress state.

$$\mathrm{M}_r = 27.06 - 0.526\theta \qquad for\ \gamma_d > 100 lb/ft^3 \tag{1}$$

$$\mathrm{M}_r = 18.18 - 0.404\theta \qquad for\ \gamma_d < 100 lb/ft^3$$

where

M_r= resilient modulus(kips/in^2)
θ = volumetric water content(%)
γ_d= dry density(lb/ft^3)

Similarly, MEPDG also presented the **Equation 2** indicating the change in resilient modulus due to the variation in the saturation or water content of the soil, as follows.

$$\log\frac{M_R}{M_{Ropt}} = a + \frac{b-a}{1+\exp\left(In\frac{-b}{a} + k_m * \left(S - S_{opt}\right)\right)} \quad (2)$$

where $\frac{M_R}{M_{Ropt}}$ resilient modulus ratio; M_R resilient modulus at a given degree of saturation; M_{Ropt} resilient modulus at a reference condition; a minimum of $\log\frac{M_R}{M_{Ropt}}$; b=maximum of $\log\frac{M_R}{M_{Ropt}}$; km=regression parameter; and $\left(S - S_{opt}\right)$= variation in degree of saturation expressed in decimals. The parameters a, b, k_m varys from coarse-grained and fine-grained materials.

For the same material, the change in its water content gives rise to the change in its soil suction, which could be observed from its soil-water characteristic curve SWCC. Past studies suggest that the soil suction has a relatively strong influence on the resilient modulus. For example, Finn et al. (1972). found the linear relationship between soil suction and its resilient modulus (Finn et al., 1972). A equation involving matric suction, axial stress, net confining stress was proposed in 1975 (Fredlund et al., 1977).

2.4 Finite element analysis of the railway transition

The calculation of the transient deformation at the certain depth of railway embankment is cumbersome by applying existing analytical formulations. In addition, some dynamic effects influence the behaviour of the embankment structure, for example, the vibration, the particle acceleration in the ballast layer, the limitation from the critical speed and response of bump that are not readily estimated. Therefore, the numerical analysis is required for the complex system simulation. There are several published studies that have conducted numerical analysis of railway transition zones. For instance, 1D and 2D dynamic models were built by Schooleman (2010) to study the influence of varying stiffness on the vertical acceleration in the transition zone with the simulated speed at 300km/h (Horníček et al., 2010). The recommendation for 2m deep cement stabilised backfill USP standard track construction has been made, and resulted from the 3-D vehicle-track dynamic simulation program (Li and Davis, 2005). A three-dimensional model with boundary conditions has been built by Gallego Giner and A López Pita (2009) to explore influences from the diverse soil with its elastoplastic behaviour. They suggested that the optimum value of slope for two types of profiles referring to the wedge applied in the embankment of the transition zone, and the requirement of filling material for the different original ground has been presented (Gallego Giner and López Pita, 2009). Seara and Gomes (2010) performed a 2D analysis in subgrade elements and found the best ratio of stiffness between two inverted transition wedges (Seara and Correia, 2010). The influence of the water Table change on the behaviour of the substructure has been examined. The result suggested that the settlement is 30 times when the ground water table increases by 50.7% at the subgrade surface (Bian et al., 2016). For the transition zone, all the related value of numerical analysis have been provided from the book *Design of Track Transition* (Read and Li, 2006).

THE FINITE ELEMENT MODEL OF STRUCTURE-EMBANKMENT TRANSITION

Soil model

The railway transition model is built as 200 m long, 35m in width, with a 7.5 m deep foundation, which is defined by Y, X, Z separately. The bridge-embankment transition with a technical solution is modelling by a three-dimensional finite element model in Figure 5, where the subsoil consisted of three sections in a longitudinal direction. From bridge end to open track, they are abutment, backfill, original ground.

This model applies the technical solution called wedge-shaped backfill, which provides a smooth transition between high stiffness of the abutment and low stiffness of the original ground. The wedge-shaped backfill between the abutment and the original ground is simulated. It is used as a technical solution of railway transition.

In terms of the geometry of the foundation along the track, the specific design of this wedge-shaped backfill applies the value of P.B. type design which refers a slope type connecting the upper end of abutment and bottom end of embankment mentioned by Gallego Giner and López Pita (2009). The slopes in abutment end and original ground end are 2:1 (horizontal to vertical). In the longitudinal direction, the length of the abutment, backfill, natural ground are 60m, 60m, 80m respectively. This profiles represents a high speed rail track model targeting at the dynamic response in the subgrade-structure system similar to that reported in past studies (Shan et al., 2013).

The open track foundation consists of three soil layers, mimicking a typical stratigraphic profile of a railway site, where the subsoil is collected and tested to perform a numerical analysis over ground vibration affecting rail deflection (Connolly et al., 2013).

Materials properties and material models

The soils, abutment, backfill, the natural ground is analysed by applying diverse models which can represent their essential stress-strain behaviour. The foundation of the open track consists of three layers. The upper layer is a 2.7 m depth silt and the second layer consisted of 3.9 m of clay. For these two top two layers, the Mohr-Coulomb model is selected. In contrast, the third layer is set to be 0.9 m thick sand, which is modelled by the hardening soil with small strain model. The hardening soil small strain model or HSS-small model is used because the vertical stress induced by train vehicles causes relatively small strain in such deep soil. The material properties of wedge-shaped backfill are in accordance with a past study (Gallego Giner and López Pita, 2009). In the proposed transition design designated as a PB type transition by Gallego Giner and López Pita (2009), the cement-treated granular material short for MGT is filled into the wedge-shaped backfill. In this paper, the Mohr-Coulomb model is selected to express the behaviour of backfill soil. An elastic, isotropic and linear model is used to reflect the properties of the bridge abutment. Table 1 summaries the material properties of subsoil used in numerical analysis.

The Mohr-Coulomb model is considered as the 'first-order' approximation of soil， which is widely used in finite element analysis of soil. It involves five input parameters, i.e. Young's modulus E and Poisson's ratio nu (ν) for soil elasticity; cohesion c, friction angle (φ) and dilatancy angle (ψ) for soil plasticity (Bentley, 2020). In PLAXIS 3D, the stiffness of certain soil layers can be defined as a constant value or increase with depth. The full Mohr-Coulomb yield condition consists of six yield functions that can be expressed in terms of three principal stresses (Smith, 2004), as shown as follows,

$$f_i = \frac{1}{2}(\sigma_2 - \sigma_3) + \frac{1}{2}(\sigma_2 + \sigma_3)\sin\varphi - c\cos\varphi \leq 0 \tag{3}$$

Where ϕ is friction angle and c is cohesion, and f_i is used to denote each individual yield function. As Mohr-Coulomb model does not take into account the stress-dependency nor stress-path dependency nor strain dependency of stiffness, the Hardening Soil model with small-strain stiffness (HSS) is selected for layers in which low strain levels are attained and these exhibit a higher stiffness than at engineering strain levels, which varies non-linearly with strain level. This model was selected to calculate the strain of three layers in the foundation because the effective stress is relatively low. From test data, sufficient agreement is found that the stress-strain curve for small strains can be adequately described by a simple hyperbolic law. The hyperbolic law can roughly describe the stress-strain curve of the HSS model, proposed by Hardin & Drnevich (1973), shown in **Equation 4**

$$\frac{G_S}{G_0} = \frac{1}{1 + \left|\frac{\gamma}{\gamma_r}\right|} \tag{4}$$

Where G_S is shear modulus, G_0 is reference shear modulus at very small strains, γ refers to strain, γ_r is threshold strain.

The linear elastic model is based on Hooke's law of isotropic elasticity. This model is used to model stiff volumes in the soil, like concrete walls or cement. In this FEA, the abutment of the bridge, which is made of concrete and reinforced material, applies the linear elastic model.

Track modelling

Geometry and configuration of the track model

The geometric properties and layers configuration of the embankment is modelled in accordance with the International Union of Railways specification (International Union of Railways, 1994) and a track model reported by Connolly et al. (2013). As Figure 6 shows, a 3D track model is built to simulate the embankment on the railway transition. The track model is determined by the isosceles trapezoid of the embankment, where the geometric parameters like upper width, bottom width, height follow the conventional railway track regulation. In the longitudinal direction, the track model is set as 200m, where the axle load moves along the track. This length ensures the moving load passes by the whole transition zone and results in a clear profile of the soil strain. The slope of the embankment is the ratio of horizontal value to vertical value, which is an essential parameter determining the stability of an embankment. Generally, it varies from site to site, according to different ground condition. In this model, the slope of 1.5:1 is used. From the bottom to the top, three layers with different height are modelled, subgrade, subballast and ballast. Ballast consisted of granular material supports the superstructure of track directly, which ensures a relatively good stiffness and permeability. It is as thick as 0.3 m. Subballast always considered as a separation between ballast and subgrade that prevent the small particles or contamination invading the subgrade, causing the deterioration of track geometry. The thickness of subballast is set at 0.2 m in this paper. At the bottom of track substructure, subgrade provides good stability of the whole embankment and its thickness is the biggest among these three layers. It is defined as 0.5 m of its thickness. The track model is built in accordance with the report targeting at the dynamic analysis of track deflection proposed as PLAXIS 3D publication (Shahraki et al., 2016).

As Figure 7 shows, there are sleepers directly installed on the formation of ballast which are then supported by the embankment,. The array of sleepers extends along the Y direction, where the interval between each sleeper is 0.6m. In the PLAXIS 3D, the sleepers are modelled as the elastic beam. Figure 7 shows the cross-section of sleepers, where the shape and size of sleepers are presented (Kaewunruen and Remennikov, 2020). The design is used to simulate the sleepers. The crosssection shows that the sleeper has the same value in width and height as 0.02 m. in the traverse direction, the sleeper as long as 0.24 m. The rails are placed following the Europe standard gauge 1.435m. It is modelled by two lines which directly contact with the train and define the path of the moving loads.

Track modulus and rail

As an essential indicator, the track modulus is considered to represent the stiffness behaviour of a whole track structure, the load-carrying capacity. In addition, the high track modulus reflects better support for the track and results in a less track deflection. Generally, beam on elastic foundation short for BOEF theory and GEOTRACK theory are two main theories used to calculate the track modulus. The beam on elastic foundation model proposed and advanced by relevant engineers and researchers (Winkler, 1867) (Timoshenko, 1921). It is defined to describe the modulus of vertical rail deflection versus the supporting force. It is classic theory to measure the rail deflection and it is assumed as a beam laying on the elastic system. Based on the BOEF model, the track modulus can be expressed by **Equation 5**, as follows,

$$\mu = -\frac{q}{\delta} \tag{5}$$

Where, μ is track modulus, δ is rail deflection, q is a function involving load, track modulus, rail modulus of elasticity, the rail moment of inertia, the distance from the load. Proposed by Chang et al. (1980), GEOTRACK model is an analytical model that incorporates all major components of the track superstructure and substructure, that is, rail, tie, fastener, ballast, subballast, and subgrade. Li et al. based on the GEOTRACK model, compared the influence of all track components on the track modulus, which is summarised by Figure 8. The numbers or letters in the Figure 8 represent the upper and lower bounds of the variables considered. The changes in track vertical lines indicate modulus caused by the change in each individual variable. Each component has upper and lower bounds of its value denoted by two points at both ends of the line from a parametric study done by Li et al. (2016). The dominant difference of track modulus caused by the change of resilient modulus of subgrade can be observed from the figure. When the resilient modulus of subgrade increases from 14 MPa to 138MPa, the track modulus has an increment of approximately 8 times. Compared with subgrade, change in stiffness of other track components have less contribution to the variation of track modulus. The material properties of ballast and subballast have relatively less influence on the track modulus, which makes a fluctuation within 5 MPa. A slight influence of the stiffness of rail fasten can be seen from this figure, as much as 15 MPa increments of track modulus. But it has a limited effect on the overall track modulus, compared with the subgrade. It could be summarised from this figure that the subgrade plays a dominant part among all track components in the track modulus and determines the track deflection directly. In this track model, the rail is not simulated, which has a limited impact on the overall track modulus and track settlement. As the behaviour of subgrade dominates the track modulus, the stiffness of subgrade is sensitive to the water content, the lack of rail has a limited effect on the result.

Track Modelling

The track model involves two types of materials, soil and beam. The beam donates the sleepers, and ballast, subballast and subgrade are considered as same features as soil. The properties of embankment layers listed by Table 2 are in accordance with the properties of the material from the PLAXIS report about dynamic load analysis of railway transition, where the data collected and tested from the high-speed rail site (Shahraki et al., 2016). Compared with the recommended values of the substructure layer proposed in a book named railway geotechnics, those values are in the normal range of their materials (Li et al., 2015). According to Li et al. (2015) research, the resilient modulus of ballast, ranging from 140 to 550 MPa, and the value 300MPa used by the simulation is within this range. Generally, the in-situ engineering properties of the material are collected and tested in the form of the specimen in the laboratory, but the existing values of these layers are applied by this finite element simulation. In the superstructure, the cohesion of clean ballast is set at 0. Both cohesion and Young's modulus is relatively important to the stress-strain calculation because the materials are modelled by the Mohr-Coulomb model. The fine-grained material is filled with the subgrade. The parameters and strength and stiffness properties used by this simulation are listed in Table 2. The properties of three embankment layers are listed by Table 2. All these layers are considered as the same features as soil or interface. The Mohr-Coulomb model generally used to describe soil strain, so it is chosen to model its stress-strain profile in this simulation. Different from the subballast and subgrade, the ballast layer consisted of the granular material essential to the track drainage. For ballast a drained condition is set as its drainage whereas for subballast and subgrade, the undrained mode is selected. In the subballast and subgrade layers, the excess pore pressure is calculated though they are above phreatic level. On the ballast surface, sleeper B70 is chosen and it is modelled by the beam type, where linear elastic denotes its feature. Table 3 lists the properties defining the sleeper. In PLAXIS 3D, the geometry of the sleeper is defined by setting its properties, including height, width, area and length. Regarding the properties of the sleeper, Young's modulus, Moment of inertia against bending around the second axis or third axis are key parameters determining the system stiffness.

Moving load modelling

Regarding the moving load applied in the track in the transition zone, an ICE train is modelled by inducing the moving point load *P* on its path. According to the technical details of the ICE train, the axle mass of this train is 16 tons, and wheel mass is 8 tons. The distance between two adjacent axles within one bogie is 2.7m, and the distance from first and last axles within one carriage is 21.7m. The dimensions of an ICE train and calculated length for the model is presented in Figure 9 (Shahraki et al., 2016). Limited by the size of the calculation profile, only one carriage of the selected train can be simulated. Four axles are simulated by four sets of moving loads to model the dynamic effect of the passenger train. The moving point load of 128kN denoting the wheel load, which is directly induced on the rail. And the train is moving forward in a velocity of 20 m/s. The technical details of the train are summarised in Table 4**.**

Role of water content in the track degradation

Relationship between moisture content and modulus of elasticity

This paper aims at exploring the role of water retention in the degradation of the railway transition zone. Young's modulus is a general parameter indicating the material stiffness and denoted by E, E_t, E_{ur} in PLAXIS 3D, which represent Young's modulus, tangent elastic modulus and resilient modulus. In this case, the resilient modulus is chosen to indicate the performance of the track during loading and unloading. However, in the PLAXIS 3D models: Mohr-Coulomb model and Hardening soil small strain model, the three stiffness related modulus are only defined as constant or linear change with depth with these two models. Given the limitation of models, the main finite element analysis is divided into two main research sections, one exploring the role of water retention in the subsoil behaviour and the other the numerical analysis of track settlement in the railway transition. Four approaches, exploring the relationship between water content and resilient modulus, are introduced. The resilient modulus calculated by four approaches is summarised by Table 7. The values are compared with the *in situ* values tested by the plate load test in a transition of the Portuguese railway line, which indicates that the resilient modulus calculated from approach 3 by Yang et al. (2005) is chosen for finite element simulation.

Approaches incorporating Resilient modulus and soil moisture content

To determine the relationship between water content and resilient modulus, the simulation compares four values of resilient modulus that result from the application of four different approaches. In this case, the wedge-shaped backfill is filled with unbound granular material short for UGM, which is calculated by four approaches proposed by previous research. The detailed procedure of calculating the resilient modulus of backfill is presented below. The result of the calculation is listed and compared by Table 7. In Table 7, a set of hydraulic scenarios is defined to simulate the seasonal change in the water content of backfill material, resulting in the variance of its resilient modulus. The analysis of four values of resilient modulus is conducted, and one group of values is selected as the input parameter of wedge-shaped backfill.

Approach 1: Resilient modulus influenced by moisture content Huang (1993)

Proposed by Huang (1993), **Equation 6** and **Equation 7** calculate the resilient modulus of subgrade soils under repeated traffic loading based on different dry density of soil. The input is water content, and output is the resilient modulus. According to the saturated dry density of backfill listed by Table 1, **Equation 7** is chosen to calculate the resilient modulus.

$$\mathrm{M}_r = 27.06 - 0.526\theta \qquad for\ \gamma_d > 100lb/ft^3 \tag{6}$$

$$\mathrm{M}_r = 18.18 - 0.404\theta \qquad for\ \gamma_d < 100lb/ft^3 \tag{7}$$

Where

M_r= resilient modulus(kips/in^2)

θ = volumetric water content(%)

γ_d= dry density(lb/ft^3)

Approach 2: Resilient modulus influenced by matric suction by Ceratti et al. (2004)

The first procedure of approach 2 is to estimate the water suction characteristic relation of soil A-7-6 based on the Van Genuchten (1980) theory. The reference of constant parameters used by Van Genuchten equation is presented. Then the equation proposed by Ceratti et al. (2004) is used to calculate the resilient modulus because the matrix suction is given. For this approach, water content, plasticity index, optimum water content, which is water content at soil maximum dry density, are required as input, and resilient can be calculated.

Step 1. Based on the Van Genuchten equation presented by **Equation 8** to get the soil suction (Van Genuchten, 1980)

$$\Theta = \frac{\theta - \theta_r}{\theta_s - \theta_r} = \left\{\frac{1}{1 + (\alpha\psi)^n}\right\}^m \quad (8)$$

Where Θ is defined as effective saturation degree. θ, θ_r, θ_s denote to the water content of the soil, the residual water content, the saturated water content. ψ is the matrix suction of soil. And n, m, α are constant parameters determined by the soil type.

Step 2. Parameters a and n for soils with different texture are listed by Table 5(after Tinjum et al., 1997, reproduced with permission).

Step 3. Use the Equation proposed by Ceratti et al., (2004)

$$M_R = 142 + 16.9(\mu_\alpha - \mu_w) \quad (9)$$

Where M_R is the resilient modulus, and $\mu_\alpha - \mu_w$ is soil suction.

Approach 3: The resilient modulus influenced by soil suction and stress state by Yang et al. (2005)

Different from approach 1 and 2, approach 3 determines the resilient modulus is deviator stress-dependent, but also include the soil suction in its equation. For the purpose of accessing the resilient modulus of backfill, the following parameter of material should be collected, water content, saturation degree and deviator stress.

Step 1: Access the soil suction of used soil according to the SWCC of UGM which is the material filled in wedge-shaped backfill, and presented in Figure 10 (Salour et al., 2015)

Step2：Soil suction to resilient modulus based on the **Equation 10** below proposed by Yang et al., (2005)

$$M_r = k_5(\sigma_d + \chi\psi_m)^{k_6} \quad (10)$$

Where k_5 and k_6 are parameters for the fitting curve, χ is saturation degree.

σ_d is deviator stress and ψ_m is matrix suction.

The deviator stress is 82kpa from the simulation result without dynamic load.

In this model, the recommended value of k_5 and k_6 are 3.04 and 0.392 (Yang et al., 2005).

χ = parameter thought to be a function of degree of saturation (χ = 0 for dry soils, χ = 1 for saturated soils)

Approach 4: subsoil resilient modulus influenced by physical state and stress state by Seed et

al. (1962)

In approach 4, the key input parameter is not only water content but also optimum water content and deviator stress in backfill layer, which is used to calculate a ratio of the current resilient modulus to the optimum resilient modulus. And the current water content can be accessed by given R.

Step.1 Prediction of fine-grained material resilient modulus based on the form of Bilinear model (Li et al., 2015), shown in **Equation 11**.

$$M_r = K_1 + K_2\sigma_d \tag{11}$$

Step.2 Calculate Mr by Rm1 considering the change of water content based on **Equation 12**, **Equation 13** (Seed et al., 1962).

$$M_r = 109000 - 1000\sigma_d \; and \; M_r = 18100 + 15.4\sigma_d \tag{12}$$

$$R_{m1} = 0.98 - 0.28(\omega - \omega_{opt}) + 0.029(\omega - \omega_{opt})^2 \tag{13}$$

Where, R_{m1} is the $M_r/M_{r(opt)}$ for the case of constant dry density. M_r is the resilient modulus at moisture content $\omega(\%)$. $M_{r(opt)}$ is the resilient modulus at maximum dry density and $\omega_{opt}(\%)$ is optimum moisture content. σ_d is deviator stress in the measured depth. The deviator stress is 82kpa from the simulation result without dynamic load.

Material properties of wedge-shaped backfill

For the estimation of resilient modulus of UGM filled in the wedge-shaped backfill, relevant stiffness properties of this material are required. In a study assessing the design and construction of the transition of railway, the investigation of transition filling material UGM was conducted, and its properties are presented in Table 6 (Li et al., 2016). The key parameters directly influence its resilient modulus are current water content, optimum water content and dry density, which are measured under compaction control. In this simulation, the calculation applies values from Li et al.(2016) without any modification because the modelling of the whole transition zone is in accordance with the in-situ construction presented by them.

3.4.4 Seasonal variation of soil moisture

Soil moisture is reported to be highly dependent on the precipitation, and it shows an obvious seasonal variance wetting and drying process over a year (Li et al., 2016). Similarly, under the track, the soil moisture content is found to be sensitive to the seasonal process of wetting and drying (Yang et al., 2005). Regardless of the drainage system in the railway, the water content in backfill material is assumed to be varied in accordance with the data of seasonal wet or dry appeared in soil moisture content investigated by Li et al. (2016). Figure 11 shows the seasonal change in volumetric soil moisture content at different depths and different distances (Li et al., 2016). The field investigation was carried out in the location with coordinate 25020 3000–25580 2200N, E103580 3700–104490 4800, resulting in a Figure indicates the volumetric soil moisture content in the time domain. The most striking aspect is the variability of water content in the time scale of four days, 10th February, 19th May, 25th August and 23th November when the data was collected. These four days roughly represented the soil state of four quarters in 2010. The seasons they are starting from Feb.10 to May. 19 is defined as dry season while from August to November is defined as wet season by Li et al. (2016). Figure 11 illustrates a marked rise of moisture content in the transition from dry season to the wet season as much as 40% of 19th May. This 50% increment or decline observed from Figure 11 can quantify the seasonal change of soil moisture of backfill material. Given that, approximately 40% of current water content of UGM that is 2% over and 2% below optimum water content for compaction are set to represent the states of soil in wet and dry seasons. The analysis of seasonal change of soil moisture content results in the four groups of water content. They are average water content 5.9%, optimum water content at maximum dry density 5.6%, water content of 3.6% which is 40% below optimum water content, water content of 7.6% which is 40% over optimum water content.

3.4.5 Resilient modulus of backfill material

To comprehensively assess how and to what extent water retention in the backfill material influences the resilient modulus, a comparison group consisting of the values of resilient modulus calculated from four different theories are compared. Additionally, the predefined water scenarios with 2% variance are set to simulate the seasonal change of water content in the soil. Table 7 compares the resilient modulus of UGM the backfill material calculated from four theories under varied water conditions. The first column shows the water conditions of the backfill material UGM is set by this study, where the average water content and optimum water content are measured by the experiments collected from the new railway line in Portugal (Paixão et al., 2013). Based on the investigation done by Li et al. where the data of seasonal change of soil moisture content reveals the 40% decline or increment happens in the subsoil (2016). Two estimated water conditions, 40% over and below optimum water content:3.6% and 7.6% are used to represent the soil physics state within the dry and wet season. Four groups of researchers are listed in the first row of the table, and each column denotes the resilient modulus calculated from their Equations, respectively. Two main criteria are used to decide a group of resilient modulus which can proceed into the finite element calculation section. The first criteria for comparison are the range of resilient modulus of UGM. The second criteria are the basic correlation that resilient modulus increase with decreasing moisture content. Addition to these two criteria, the sensitivity to the water content is also essential to the clarity of the simulation result, which means an obvious soil displacement due to different resilient modulus. In the cyclic load triaxial tests are done by Paixão et al. (2013), the resilient modulus of UGM was suggested to vary from 50MPa to 150Mpa along the transverse direction. However, for the subsoils of open track, the resilient modulus at optimum water content ranges from 20Mpa to 100Mpa. Based on these criteria, the resilient modulus in the column of the Huang (1993) method is over the range of UGM, and it also does not show a clear sensitivity to the change of water content. Values from Ceratti et al. (2004) and Seed et al. (1962). are lower than the range of resilient modulus of UGM, while these two approaches meet in the range of resilient modulus of subsoil. Different from the other three approaches where the maximum resilient modulus happens at the lowest water content, the maximum resilient modulus at the optimum water content in the Seed 1962 approach. The experimental Equation proposed by Yang et al. (2005) gives a reasonable set of resilient modulus that meets the categories described in the criteria. Moreover, this set of data shows good sensitivity to water content, so the values in Yang et al. (2005) column are selected as the resilient modulus indicating the stiffness of backfill material, which is essential to the calculation of soil displacement in the next section.

RESULTS AND DISCUSSION

Water retention influence on the track degradation

This numerical analysis is carried out to explore the role of water retention in the track degradation within the transition between the bridge abutment and open track embankment. The railway transition model, including bridge abutment, the wedged-shape backfill and open track embankment is designed. Based on the developed transition model, the settlement is compared under three water conditions where water retention in backfill generally increases as ω=3.6%, ω=5.6%, ω=7.6%. This finite element analysis mainly observes how the soil behaviour of backfill in transition change with varied moisture content. To be specific, the result only outputs as displacement μ in the unit of mm, but in discrete and continuous forms. The discrete output is Figures of the displacement of selected stress points. The stress point displacement is plotted versus the dynamic time. The unit of X axle is day instead of second, which is limited to the PLAXIS 3D.

Both the discrete and continuous result is analysed and compared under hydraulic conditions that the effect of water retention of backfill on the track differential settlement can be observed.

Soil displacement

Along the central line at X=11 of the finite element model of railway transition, the stress points of interest are selected and distributed according to different purposes. In the longitudinal direction, from the end of the model, the bridge abutment starts from Y=0 and ends at Y=60. From Y=60 to Y= 120, there is the wedge-shaped backfill which is constructed to provide a smooth transition from high stiffness of abutment to the natural ground of open track. Connected to the backfill, the open track extends from Y=120 to Y=200, which is another end of the model. In the time domain, and the train simulated in this study has the speed of 20m/s. From t=1s to t=3s, the train load is applied in the bridge abutment, when t=3s, the train is entering the wedge-shaped backfill. From 3 s, the train is passing the backfill section until 6s. After t=6s, the train runs over open track and stop at t=10s.

As a summary, 1 to 3s is the abutment, 3s to 6s is backfill, 6s to 10s is the open track. The coordinates of the stress points of interest are summarised in Appendix A.

Appendix D illustrates the soil displacement in the formation in the time domain within water content of 3.6%, 5.6%, 7.6% when T=6s.

Effect of moisture content on the degradation

In order to observe the differential deformation of ballast within the transition zone, the first measurement of soil displacement is done and denoted by A, B, C. Point A, B, C are located in the bridge abutment, wedge-shaped backfill and open track ground respectively. Figure 12 illustrates the locations of point A, point B and point C. These three points lay on the surface of ballast at the same level in Z=1 plane, which distributes along the central line of the track in the X=11 line. Differently, point A lays on the abutment section with Y=23.8, and point B is assigned in the backfill section with Y=72.3, while the point C locates on the open track embankment section with Y=168.4.

To investigate the effect of reducing the moisture content on the ballast settlement in the transition, the maximum total strain of ballast among three water conditions are compared in Table 4.1. Under the moisture content ω =3.6%, 5.6%, 7.6%, the strain of stress point A, B, C are separately plotted in Figure 13**.** In Figure 13**,** the difference in strain starts to appear from t=3s, and peaks at t=5s. This is the time when the second axle just passed point A, and the strain reaches its maximum. The maximum value for ω = 3.6% is -3.8mm, and -0.099mm for ω= 7.6%, and -0,114mm for ω = 5.6%. In Figure 13, the variance happens at t=5s and peaks at 7s. The maximum strain for ω= 7.6% is -7mm, for ω= 3.6% is -0.35mm, for ω= 5.6% is -0.29mm. Figure 13 shows the significant difference in the strain at t=10s. The maximum strain for ω= 7.6% is -15mm, for ω= 5.6% is -1.17mm，for ω= 3.6% is -0.91mm. Comparing two water conditions in the transition which are wet season ω= 7.6% and dry season ω= 3.6%, the ballast settlement in bridge abutment section can be reduced by 97.39%. The ballast strain reduction in the backfill section is up to 95.00%, and 93.93% strain reduction in the open track section. It is possible to hypothesize that reducing moisture content is likely to have a greater effect on the stiffer material.

To investigate the effect of moisture content on track degradation, the degree of degradation is compared among three water conditions (Figure 14). This figure indicate that larger strains are obtained for the section of open track, and subsequently lower strain are obtained for backfill, and abutment. More important is the obvious difference in degradation observed in Figure 14. The differential settlement under three water condition is summarised in

Table 9, where ε_A ε_B ε_C denotes the strain of stress point A, B and C or strain in abutment backfill and open track respectively. In this study, the deviance of soil strain from the adjacent sections is calculated, which is different from the parameter standard deviation short for SD, measured by mid chord offset short for MCO proposed by Carr et al. (2003). There is an obvious correlation between soil moisture content and track degradation can be observed from

Table 9, where the successive increases in the differential settlement are observed for higher moisture contents. These results suggest that reducing moisture content can mitigate track degradation in the transition zone. These results corroborate the findings of a great deal of the previous work which consider and soil-water relation are the key primary causes of track degradation at the transition (Kerr and Moroney, 1995) (Li and Davis, 2005) (Nicks, 2009) (Gallage et al., 2013b).

Effect of moisture content on the settlement of track layers

For comparing the settlement of ballast, subballast and subgrade within the transition section, the measurement of soil displacement is done under three moisture state of backfill material. Figure 15 illustrates the location of measuring point D, E, F. From the cross-section A-A* in the Figure of track embankment in Figure 15, point D, E, F are selected to represent the stress points laying on each track layer in the finite element model. The measurement of the settlement of each track layer can be done. Point D is on the interface between ballast and subballast with level Z=0.7. Point E lays on the interface between subballast and subgrade at Z=0.5, while point F on the formation which is Z=0. These three points lay in the same cross-section of the model, which is the plane Y=72.3. This is the plane where wedge-shaped backfill supports the track. It can be observed from the Figure that three points sit on the central line at X=11of the model. The coordinates of the stress points of interest are summarised in Appendix A.

To compare the settlements of track layers, the case of stress point DEF under ω=3.6% is examined. Figure 16 illustrates the strain of track layers: ballast, subballast and subgrade denoted by stress points D, E, F, in the time domain. The strain of track layers peaks at around 3s. It can be clearly observed from the figure that, in this finite element model, the strain of ballast is higher than subballast and subgrade. The subgrade strain is slightly higher than the subballast. This result is In accordance with the present experimental result demonstrated that settlement of ballast generally is greater than other layers in the track substructure (Li et al., 2015). However, the strain distribution in the track substructure is site-dependent or model-dependent.

The strain in substructure layers under ω= 3.6% peaks at t=3s, while the strain in substructure layers under ω= 7.6% peaks at t=4s. An assumption can be made that lower water content leads to a faster response of strain. This slower response could be attributed to the lower modulus of elasticity resulted from higher moisture content. Figure 16 illustrates the strain of ballast, subballast and subgrade separately in the order of ω= 3.6%, ω= 5.6%, ω= 7.6%. The maximum strain of each layer under three water conditions is summarized in

Appendix B. The effect of water content could be quantified by measuring the reduction of strain. Comparing the case of ω= 3.6% and ω= 7.6%, the reduction in the strain of ballast is 71.2%. The strain in subballast reduces by 70.7% and there is a reduction of 62.8% in subgrade strain. There are two possible explanation for these results. Compared with subballast and subgrade, the material with higher stiffness (i.e. ballast) performance could be benefited from the effect of reducing moisture content. In addition, it is likely that the effect of moisture content is likely to decrease with depth. In

Appendix B**,** the strain of subballast is lower than subgrade strain under ω= 3.6%, while subballast strain is higher than subgrade under ω= 7.6%. This finding is unexpected and suggests that maybe subballast is more sensitive than subgrade to change of moisture content in the transition.

Effect of moisture content on the settlement variation with depth

To assess the effect of moisture content on the settlement of wedge-shaped backfill with varied depth, three stress points denoted by point G, point H and point I are selected to present a profile of settlement of backfill material UGM vary with depth. Figure 18 shows the location of measuring point G, H and I. Measurement targets the soil displacement in the backfill, so plane Y=72.3 is selected. And all the measuring points lay on the central line X=11 of the model. These three measuring points locate in the wedge-shaped backfill, which is a technical solution applied in the railway foundation. Under the formation at Z=0, there are point G, point H and point with -2.5m, -5m, -7.5m in depth.

Figure 19 illustrates the strain of backfill with the depth of 2.5m, 5m, and 7.5m under ω= 3.6%, ω= 5.6%, ω= 7.6%. The irregularity can be observed that the maximum values happen at different times. However, in the G and H profiles, high moisture content case ω= 7.6% reach its maximum strain slower than the dry case ω= 3.6%.

Appendix C summarises the maximum strain of backfill with varied depth under three water conditions. Regardless of the water condition, the basic trend is that the strain decreases with depth. This is mainly due to a reduction in effective stress with depth. There is a reduction of 77.2% and 62.3% in the depth of 2.5m and 5m respectively when the moisture content reduces from 7.6% to 3.6%. The results also suggest that moisture content might have a weaker effect on the soil strain at higher depths.

The soil displacement along the track

For the purpose of assessing the effect of water content in the transition on the degradation, the soil displacement and Young's modulus along the measuring alignment are plotted in Error! Reference source not found. and Figure 20 separately**.** Regarding the foundation, the significant soil settlement happens on the top of the foundation or formation rather than deeper soil. The measuring alignment is a line lying on the formation in the vertical direction and on the centre of track gauge in the horizontal direction. It extends through the transition model with the coordinate of X=11 and Z=0. Figure 20 presents the overall Young's modulus of the transition model under ω= 3.6%, 5.6%,7.6%. The modulus of elasticity of foundation with multilayers can be estimated by **Equation 14** and is widely used by some researchers to estimate the overall modulus of elasticity of the layered soil (Connolly et al., 2014) (Brahma and Mukherjee, 2010) (Wang and Cao, 2013).

$$E_{eq} = \frac{\sum H_i E_i}{\sum H_i} \tag{14}$$

Where, E_{eq} is the equivalent Young's modulus, H_i is layer thickness, E_i is layer young's modulus. The comparison among three moisture content results in the three similarly shaped straight lines from top to bottom. Compared the cases of moisture content of 3.6% and 7.6%, the difference between these two cases gradually starting from 30m and reaches its peak of 80MPa at around 70m. High moisture content in the backfill leads to the low overall Young's modulus of the transition, vice versa. The gap showed in the Figure suggests that the moisture content of backfill plays an important role in the overall modulus of elasticity of the transition zone. Considering the case of a railway bridge approach, the sudden oscillation always happens when the train passes from bridge abutment to the embankment (Nicks, 2009) (Woodward et al., 2014). The moisture content of 3.6% can provide the best transition in stiffness passing from abutment to wedge-shaped backfill among three cases. It can therefore be assumed that reducing the water content of the technical solution such as wedge-shaped backfill may mitigate the bump in the structure-embankment approach. However, from 90m to 150m, three cases converge at the low value of Young's modulus. The lower water content shows a less smooth transition in stiffness, limited by the low stiffness of the open track section where the track system lays on the natural ground. But it seems not to result in the sudden differential settlement in a short segment of track, compared with the bump in the bridge approach. Therefore, it is possible that the lower moisture content in the backfill section can mitigate the bump from abutment to backfill, but it may result in the greater instability of settlement from backfill to the open track. Figure 21 shows the soil displacement of the formation in the unit of mm and three soil displacement profile is plotted under the moisture content of ω= 3.6%, 5.6%,7.6%. It is apparent from the Figure that there is a significant fluctuation in each profile of displacement. A possible explanation for the successive fluctuations might be the moving load modelling. As Figure 9 shown, the moving loads are not induced continuously but induced by an interval of 21.7m, which leads to the successive and growing peak of waves in the displacement profile. Due to the gradually decreasing overall modulus of elasticity of subsoil, there is a clear trend of increasing displacement can be observed in three cases. From 0m to 120m, the case of 3.6% moisture content results in relatively fewer fluctuations and lower displacement in the abutment and backfill sections, compared with the case of the wet season. At least, in this model, the lower water content of backfill can mitigate the degradation in the transition zone but not include the open track section. Three cases reach the same peak value of displacement of 27mm in this simulation, it is due to the constant Young's modulus of the natural ground under the open track. Differently, the severe fluctuations still exist in the case ω= 7.6% which Regularly oscillates at a certain frequency. The case ω= 3.6% appears to be relatively stable when it approaches its peak. Although they share the same maximum displacement, lower water content has a positive effect on the smoothing the track geometry in the vertical direction. Therefore, it is possible to assume that smooth railway geometry in the open track section within the transition can be reached by reducing the water content in the backfill material, but no help in reducing the maximum displacement.

CONCLUSIONS

The simulation results indicate that there is a clear correlation between water retention and track degradation in the railway bridge-embankment transition. The software PLAXIS 3D was used to develop the transition model. Except for the track and soil and bridge structure, the wedge-shaped backfill filled with reinforcement material UGM is included by the model. The water content of subsoil in the transition is an independent variable in the simulation. The seasonal change in water content of subsoil is mainly considered, which is set into three cases, they are wet season water content ω= 7.6%, current water content ω= 5.6% and dry season water content ω= 3.6%. Among the three cases, the lowest moisture content ω= 3.6% resulted in the lowest track settlement. The comparison between three cases suggests that low water content has a significant reduction in the soil strain. The results indicated that this effect of reduction is greater when the material is stiffer and less significant for larger depths. According to the comparison between three cases of settlement profile along the track, the bump from the bridge structure to backfill can be mitigated and smooth track geometry in the backfill and the open track can be achieved by reducing water content. Considering the time, the soil in lower water content shows a quicker response to the stress than high water content. The subballast seems to be more sensitive than subgrade to change of moisture content in the transition. Some of the displacement data obtained for the case ω= 7.6%, exceeded the expected service range (i.e. lower than 10mm). This is likely due to a limitation of

PLAXIS3D which cannot fully simulate the continuous moving loads induced on the model.

Finally, while this study shows that performance gains in terms of track degradation are achieved by controlling the water content in the transition zone, due caution should be exercises as the hydraulic water conditions and moving load dynamic analysis cannot be fully coupled in the model presented in this paper.

REFERENCES

Bentley 2020. *PLAXIS Material Model Manual* [Online]. Bentley. Available from: https://communities.bentley.com/cfs-file/__key/communityserver-wikis-components-files/00-00-00-05-58/0118.PLAXIS3DCE_2D00_V20.02_2D00_3_2D00_Material_2D00_Models.pdf.

Bian, X., Jiang, H., Chen, Y. and Connolly, D.P. 2016. Preliminary testing on high-speed railway substructure due to water level changes. *Procedia engineering*. **143**, pp.769–781.

Brahma, P. and Mukherjee, S. 2010. A realistic way to obtain equivalent Young's modulus of layered soil *In*: *Indian geotechnical conference. Bombay, India.*, pp.305–308.

Carr, G.A., Diaz, C. and Bloom, J. 2003. *Method and apparatus for track geometry measurement*. Google Patents.

Ceratti, A.J., Gehling, W.Y.Y. and Núñez, W.P. 2004. Seasonal variations of a subgrade soil resilient modulus in southern Brazil. *Transportation Research Record*. **1874**(1), pp.165–173.

Chang, C.S., Adegoke, C.W. and Selig, E.T. 1980. GEOTRACK model for railroad track performance. *Journal of Geotechnical and Geoenvironmental Engineering*. **106**(11).

Connolly, D., Giannopoulos, A. and Forde, M.C. 2013. Numerical modelling of ground borne vibrations from high speed rail lines on embankments. *Soil Dynamics and Earthquake Engineering*. **46**, pp.13–19.

Connolly, D., Kouroussis, G., Giannopoulos, A., Verlinden, O., Woodward, P. and Forde, M. 2014. Assessment of railway vibrations using an efficient scoping model.

Culley, R.W. 1971. Effect of freeze–thaw cycling on stress–strain characteristics and volume change of a till subjected to repetitive loading. *Canadian Geotechnical Journal*. **8**(3), pp.359–371.

Dhir, R.K., de Brito, J., Silva, R.V. and Lye, C.Q. 2019. 11 - Use of Recycled Aggregates in Geotechnical Applications *In*: R. K. Dhir, J. de Brito, R. V. Silva and C. Q. Lye, eds. *Sustainable Construction Materials* [Online]. Woodhead Publishing, pp.419–450. Available from: http://www.sciencedirect.com/science/article/pii/B978008100985700011X.

Drumm, E.C. and Meier, R. 2003. *LTPP Data Analysis: Daily and Seasonal Variations in Insitu Material Properties*. Transportation Research Board, National Research Council.

Edil, T.B. and Motan, S.E. 1979. Soil-water potential and resilient behavior of subgrade soils. *Transportation Research Record*. (705).

Elfino, M.K. and Davidson, J.L. 1989. Modeling field moisture in resilient moduli testing *In*: *Resilient moduli of soils: laboratory conditions*. ASCE, pp.31–51.

Finn, F.N., Nair, K. and Monismith, C.L. 1972. Applications of theory in the design of asphalt pavements *In*: *Presented at the Third International Conference on the Structural Design of Asphalt Pavements, Grosvenor House, Park Lane, London, England, Sept. 11-15, 1972.*

Fredlund, D.G., Bergan, A.T. and Wong, P.K. 1977. Relation between resilient modulus and stress conditions for cohesive subgrade soils. *Transportation Research Record*. (642).

Gallage, C., Dareeju, B. and Dhanasekar, M. 2013a. *State-of-the-art : track degradation at bridge transitions*. Proceedings of the 4th International Conference on Structural Engineering and Construction Management 2013.

Gallage, C., Dareeju, B. and Dhanasekar, M. 2013b. *State-of-the-art : track degradation at bridge transitions*.

Gallego Giner, I. and López Pita, A. 2009. Numerical simulation of embankment—structure transition design. *Proceedings of the Institution of Mechanical Engineers, Part F: Journal of Rail and Rapid Transit*. **223**(4), pp.331–343.

Gallego, I., Snchez-Cambronero, S. and Rivas, A. 2012. Criteria for Improving the Embankment-Structure Transition Design in Railway Lines *In*: X. Perpinya, ed. *Infrastructure Design, Signalling and Security in Railway* [Online].

Hardin, B.O. and Drnevich, V.P. 1973. 35. Shear modulus and damping: equations and curves: B. O. Hardin and V. P. Drnevich.Proceedings of the American Society of Civil Engineers; Journal of the Soil Mechanics and Foundation Division, 98 (SM7), 667–692 (1972); 23 ref., 16 fig. *Journal of Terramechanics*. **9**(2), p.102.

Horníček, L., Tyc, P., Lidmila, M., Krejčiříková, H., Jasanský, P. and Břešt?'ovský, P. 2010. An investigation of the effect of under-ballast reinforcing geogrids in laboratory and operating conditions. *Proceedings of the Institution of Mechanical Engineers, Part F: Journal of Rail and Rapid Transit*. **224**(4), pp.269–277.

Huang, Y.H. (Yang H. 1993. *Pavement analysis and design*. Englewood Cliffs, NJ: Prentice Hall.

International Union of Railways 1994. *UIC code 719R: earthworks and track layers for railway lines*. Paris, France.

Kaewunruen, S. and Remennikov, A. 2020. Relationship between impact energy and fracture toughness of prestressed concrete railway sleepers. *Faculty of Engineering - Papers*.

Kennedy, J., Woodward, P.K., Medero, G. and Banimahd, M. 2013. Reducing railway track settlement using three-dimensional polyurethane polymer reinforcement of the ballast. *Construction and Building Materials*. **44**, pp.615–625.

Kerr, A. and Moroney, B. 1995. *Track Transition Problems and Remedies* [Online].

Kodikara, J. and Yeo, R. 2015. Chapter 6 - Performance Evaluation of Road Pavements Stabilized In Situ *In*: B. Indraratna, J. Chu and C. Rujikiatkamjorn, eds. *Ground Improvement Case Histories* [Online]. Butterworth-Heinemann, pp.165–203.

Li, D. and Davis, D. 2005. Transition of railroad bridge approaches. *Journal of Geotechnical and Geoenvironmental Engineering*. **131**(11), pp.1392–1398.

Li, D., Hyslip, J., Sussmann, T. and Chrismer, S. 2015. *Railway geotechnics*. CRC Press.

Li, D. and Selig, E.T. 1994. Resilient modulus for fine-grained subgrade soils. *Journal of geotechnical engineering*. **120**(6), pp.939–957.

Li Dingqing and Davis David 2005. Transition of Railroad Bridge Approaches. *Journal of Geotechnical and Geoenvironmental Engineering*. **131**(11), pp.1392–1398.

Li, S., Birk, S., Xue, L., Ren, H., Chang, J. and Yao, X. 2016. Seasonal changes in the soil moisture distribution around bare rock outcrops within a karst rocky desertification area (Fuyuan County, Yunnan Province, China). *Environmental Earth Sciences*. **75**(23), p.1482.

Liang, R.Y., Rabab'ah, S. and Khasawneh, M. 2008. Predicting moisture-dependent resilient modulus of cohesive soils using soil suction concept. *Journal of Transportation Engineering*. **134**(1), pp.34–40.

Mishra, D., Qian, Y., Huang, H. and Tutumluer, E. 2014. An integrated approach to dynamic analysis of railroad track transitions behavior. *Rail Geomechanics - From Theory to Practice*.

1(4), pp.188–200.

Nicks, J. 2009. The Bump at the End of the Railway Bridge.

Olidid, C. and Hein, D. 2004. Guide for the mechanistic-empirical design of new and rehabilitated pavement structures *In*: *2004 Annual conference and exhibition of the Transportation Association of Canada-Transportation Innovation-accelerating the pace*.

Paixão, A., Fortunato, E. and Calçada, R. 2013. Design and construction of backfills for railway track transition zones. *Proceedings of the Institution of Mechanical Engineers, Part F: Journal of Rail and Rapid Transit*. **229**(1), pp.58–70.

Read, D. and Li, D. 2006. Design of track transitions. *TCRP Research Results Digest*. (79).

Robnett, Q.L. and Thompson, M.R. 1976. Effect of lime treatment on the resilient behavior of fine-grained soils. *Transportation Research Record*. **560**(1), pp.1–20.

Salour, F., Erlingsson, S. and Zapata, C. 2015. Model for Seasonal Variation of Resilient Modulus in Silty Sand Subgrade Soil. *Transportation Research Record: Journal of the Transportation Research Board*. **2510**, pp.65–73.

Sañudo, R., dell'Olio, L., Casado, J.A., Carrascal, I.A. and Diego, S. 2016. Track transitions in railways: A review. *Construction and Building Materials*. **112**, pp.140–157.

Sauer, E.K. and Monismith, C.L. 1968. Influence of soil suction on behavior of a glacial till subjected to repeated loading. *Highway Research Record*. (215).

Seara, I. and Correia, A.G. 2010. PERFORMANCE ASSESMENT SOLUTIONS FOR TRANSITION ZONES EMBANKMENT-BRIDGE RAILWAYS TROUGH NUMERICAL SIMULATION 3D. , p.2.

Seed, H.B., Chan, C.K. and Lee, C.E. 1962. Resilience characteristics of subgrade soils and their relation to fatigue failures in asphalt pavements *In*: *International Conference on the Structural Design of Asphalt Pavements. SupplementUniversity of Michigan, Ann Arbor*.

Seed, H.B., Mitry, F.G., Monismith, C.L. and Chan, C.K. 1967. Prediction of flexible pavement deflections from laboratory repeated-load tests. *NCHRP report*. (35).

Shahraki, M., Sadaghiani, M.R.S. and Witt, T. 2016. *3D Modelling of Train Induced Moving Loads on an Embankment* [Online]. Bentley. Available from: https://communities.bentley.com/products/geotech-analysis/w/plaxis-soilvision-wiki/45475/3d-modelling-of-train-induced-moving-loads-on-an-embankment.

Shan, Y., Albers, B. and Savidis, S.A. 2013. Influence of different transition zones on the dynamic response of track–subgrade systems. *Computers and Geotechnics*. **48**, pp.21–28.

Smith, I.M. (Ian M. 2004. *Programming the finite element method* Fourth edition. Chichester: Wiley.

Timoshenko, S.P. 1921. LXVI. On the correction for shear of the differential equation for transverse vibrations of prismatic bars. *The London, Edinburgh, and Dublin Philosophical Magazine and Journal of Science*. **41**(245), pp.744–746.

Tinjum, J.M., Benson, C.H. and Blotz, L.R. 1997. Soil-water characteristic curves for compacted clays. *Journal of geotechnical and geoenvironmental engineering*. **123**(11), pp.1060–1069.

Van Genuchten, M.T. 1980. A closed-form equation for predicting the hydraulic conductivity of unsaturated soils 1. *Soil science society of America journal*. **44**(5), pp.892–898.

Varandas, J., Paixão, A., Fortunato, E., Hölscher, P. and Calçada, R. 2014. Numerical Modelling of Railway Bridge Approaches: Influence of Soil Non-Linearity. *The International Journal of Railway Technology*. **3**, pp.73–95.

Wang, Y. and Cao, Z. 2013. Probabilistic characterization of Young's modulus of soil using equivalent samples. *Engineering Geology*. **159**, pp.106–118.

Winkler, E. 1867. *Die Lehre von der Elasticitaet und Festigkeit: mit besonderer Rücksicht auf ihre Anwendung in der Technik für polytechnische Schulen, Bauakademien, Ingenieue, Maschinenbauer, Architecten, etc*. Dominicus.

Woodward, P., Laghrouche, O. and El-Kacimi, A. 2014. Railway track transition dynamics and reinforcement using polyurethane GeoComposites. *Geotechnical Engineering*. **45**(1), pp.28–38.

Yang, S.-R., Huang, W.-H. and Tai, Y.-T. 2005. Variation of resilient modulus with soil suction for compacted subgrade soils. *Transportation Research Record*. **1913**(1), pp.99–106.

List of Figures:

Figure 1. Comparison of track settlements from 4 sites (modified after Li and Davis, 2005) 45

Figure 2. Schematic diagram of possible failures and issues in a bridge transition (after Gallage et al., 2013, reproduced with permission)..........45

Figure 3. Relationship between *Mr* and *w* with water content difference, w_{opt} = optimum water content (modified after Seed et al., 1962)..........46

Figure 4 Resilient modulus of subgrade soils under repeated traffic loading (after Huang, 2004, reproduced with permission)..........47

Figure 5 The geometry of the transition model..........47

Figure 6. The configuration of the track model..........48

Figure 7 The geometry of sleepers modelled..........48

Figure 8 Effects of track component properties on track modulus (after Li et al. 2016, reproduced with permission)..........49

Figure 9 The Dimensions of an ICE train (after Shahraki et al., 2016, reproduced with permission) 49

Figure 10. SWCC of subgrade soil (modified after Salour et al., 2015)..........49

Figure 11. Seasonal change in volumetric soil moisture content at the different depths (after Li et al., 2016, reproduced with permission)..........50

Figure 12. The location of measuring point ABC..........50

Figure 13. The ballast strain under ω= 3.6%, 5.6%,7.6% in the abutment, backfill and open track .51

Figure 14. The ballast strain of stress points A, B, C under ω= 3.6%, 5.6%,7.6% separately...........52

Figure 15. The cross-section A-A* and location of measuring point DEF..53

Figure 16 The strain of ballast, subballast and subgrade under ω=3.6%..53

Figure 17 The strain of substructure layers under ω= 3.6%, 5.6%,7.6%..54

Figure 18 The location of measuring point GHI..55

Figure 19 The strain of backfill material varying with depth under ω= 3.6%, 5.6%,7.6%. 56

Figure 20The Young's modulus of subsoil under ω= 3.6%, 5.6%,7.6%..56

Figure 21 The displacement of the formation along the track under ω= 3.6%, 5.6%,7.6% 57

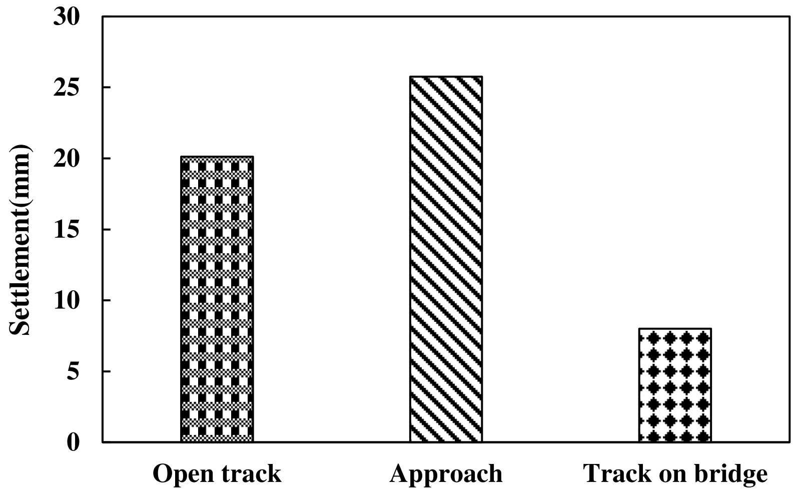

Figure 1. Comparison of track settlements from 4 sites (modified after Li and Davis, 2005)

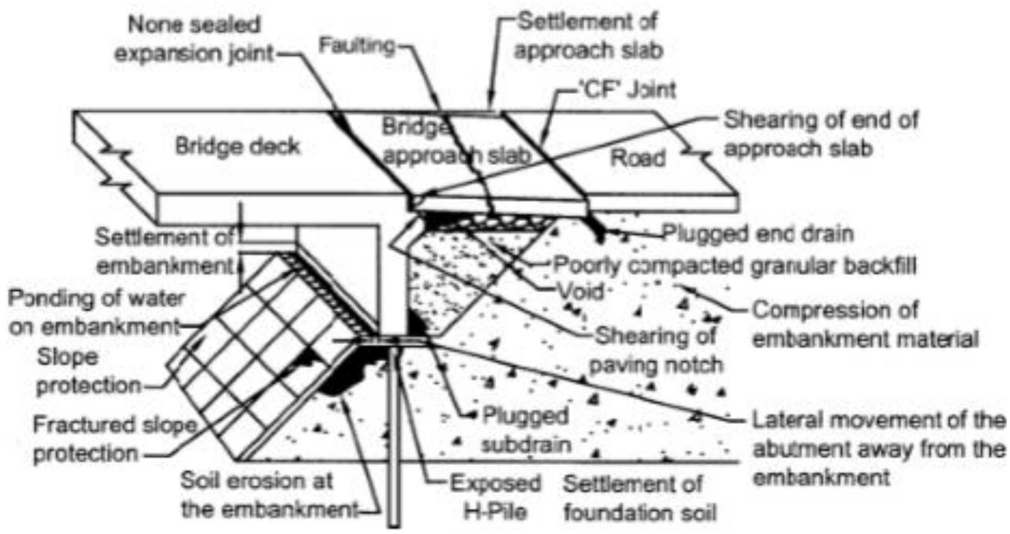

Figure 2. Schematic diagram of possible failures and issues in a bridge transition (after Gallage et al., 2013, reproduced with permission)

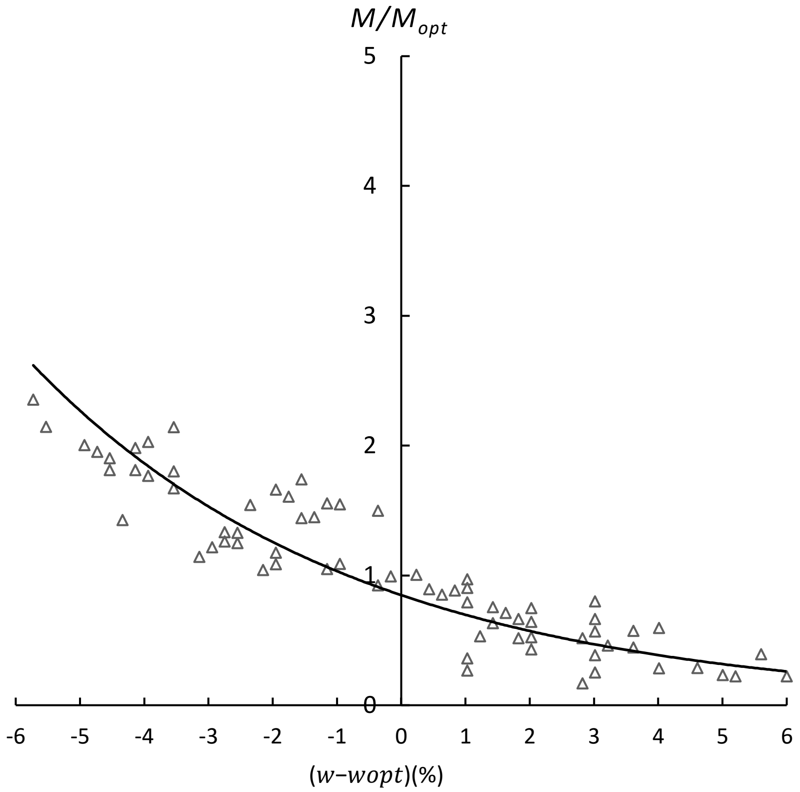

Figure 3. Relationship between Mr and w with water content difference, w_{opt} = optimum water content, M = resilience modulus, M_{opt}=resilience modulus at optimum water content (modified after Seed et al., 1962)

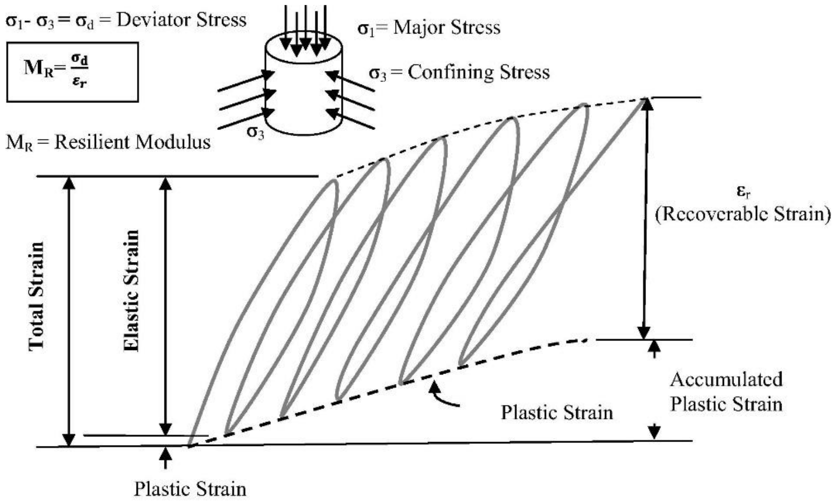

Figure 4 Resilient modulus of subgrade soils under repeated traffic loading (after Huang, 2004, reproduced with permission)

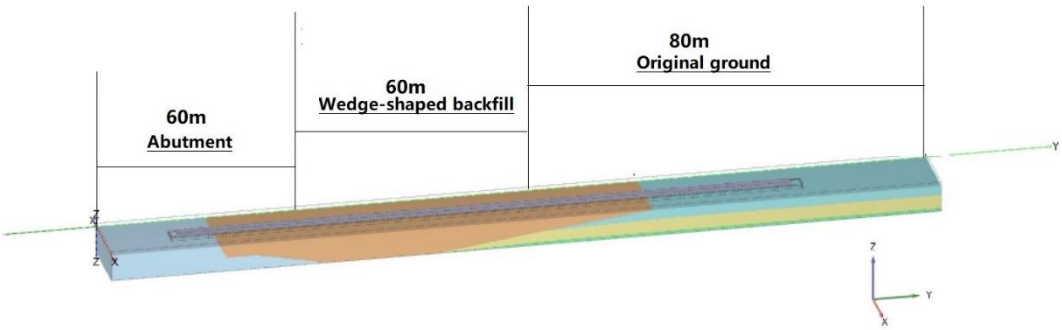

Figure 5 The geometry of the transition model

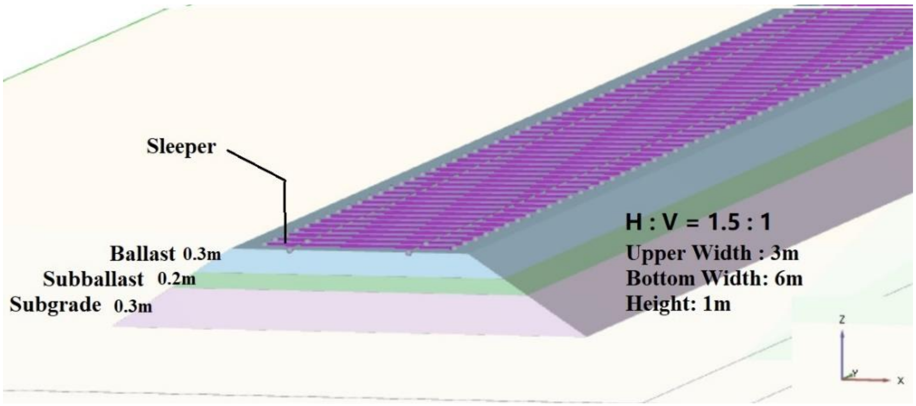

Figure 6. The configuration of the track model

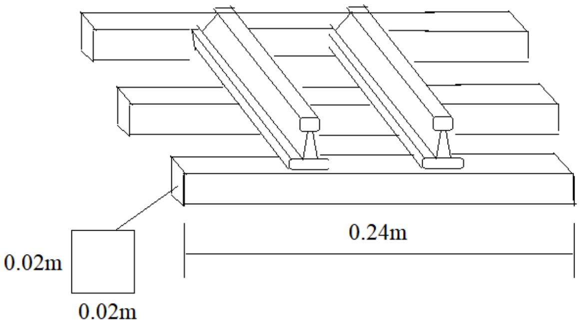

Figure 7 The geometry of sleepers modelled

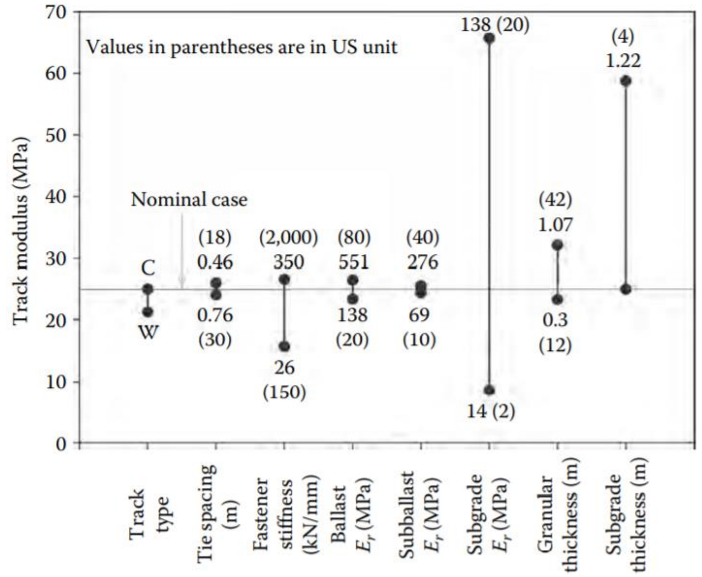

Figure 8 Effects of track component properties on track modulus (after Li et al. 2016, reproduced with permission)

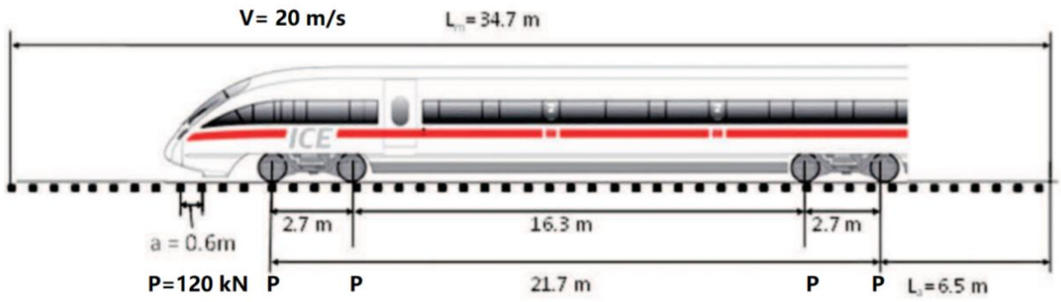

Figure 9 The Dimensions of an ICE train (after Shahraki et al., 2016, reproduced with permission)

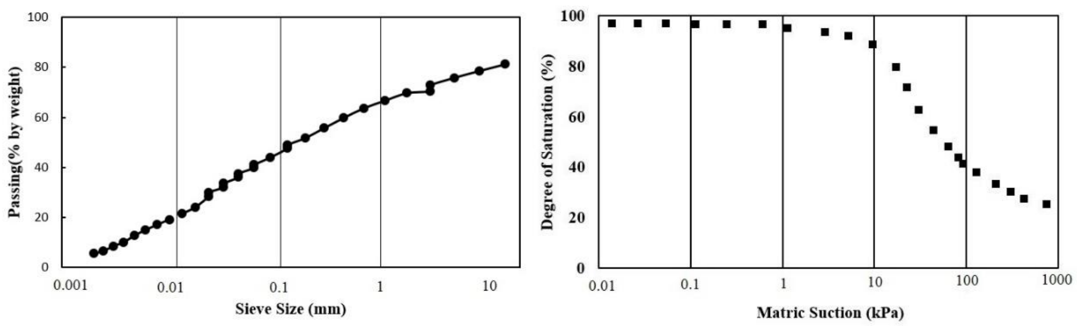

Figure 10. SWCC of subgrade soil (modified after Salour et al., 2015)

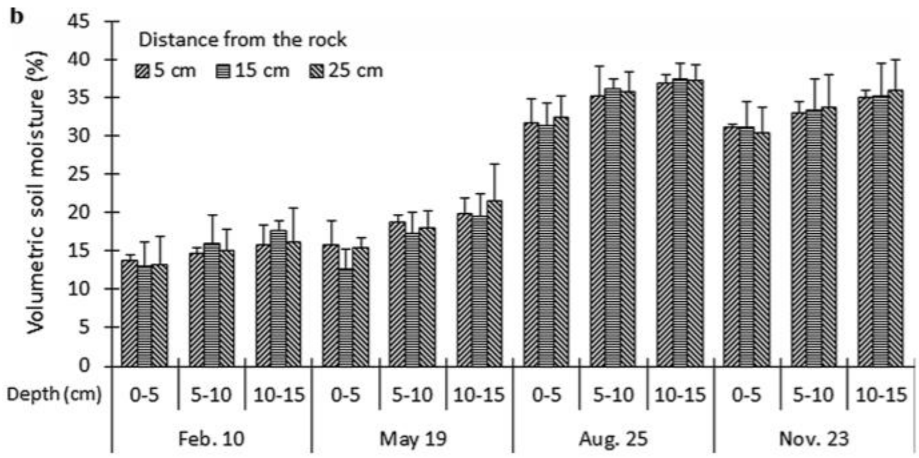

Figure 11. Seasonal change in volumetric soil moisture content at the different depths (after Li et al., 2016, reproduced with permission)

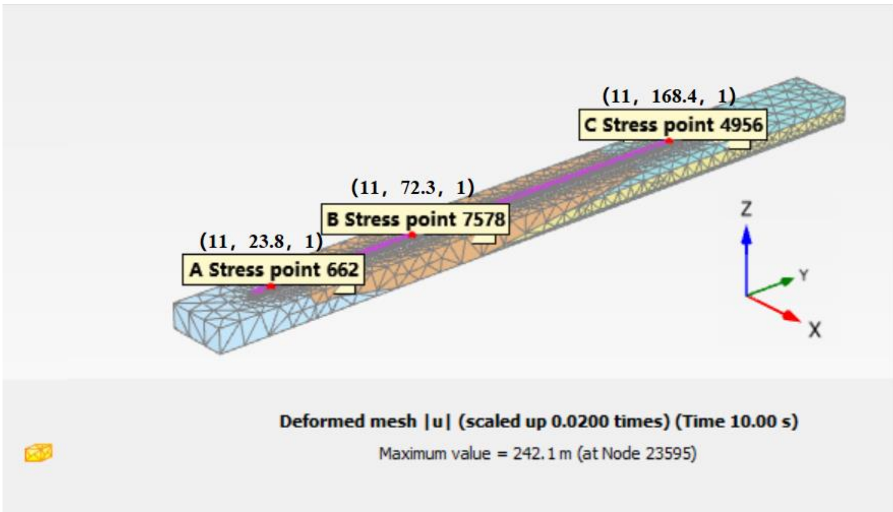

Figure 12. The location of measuring point ABC

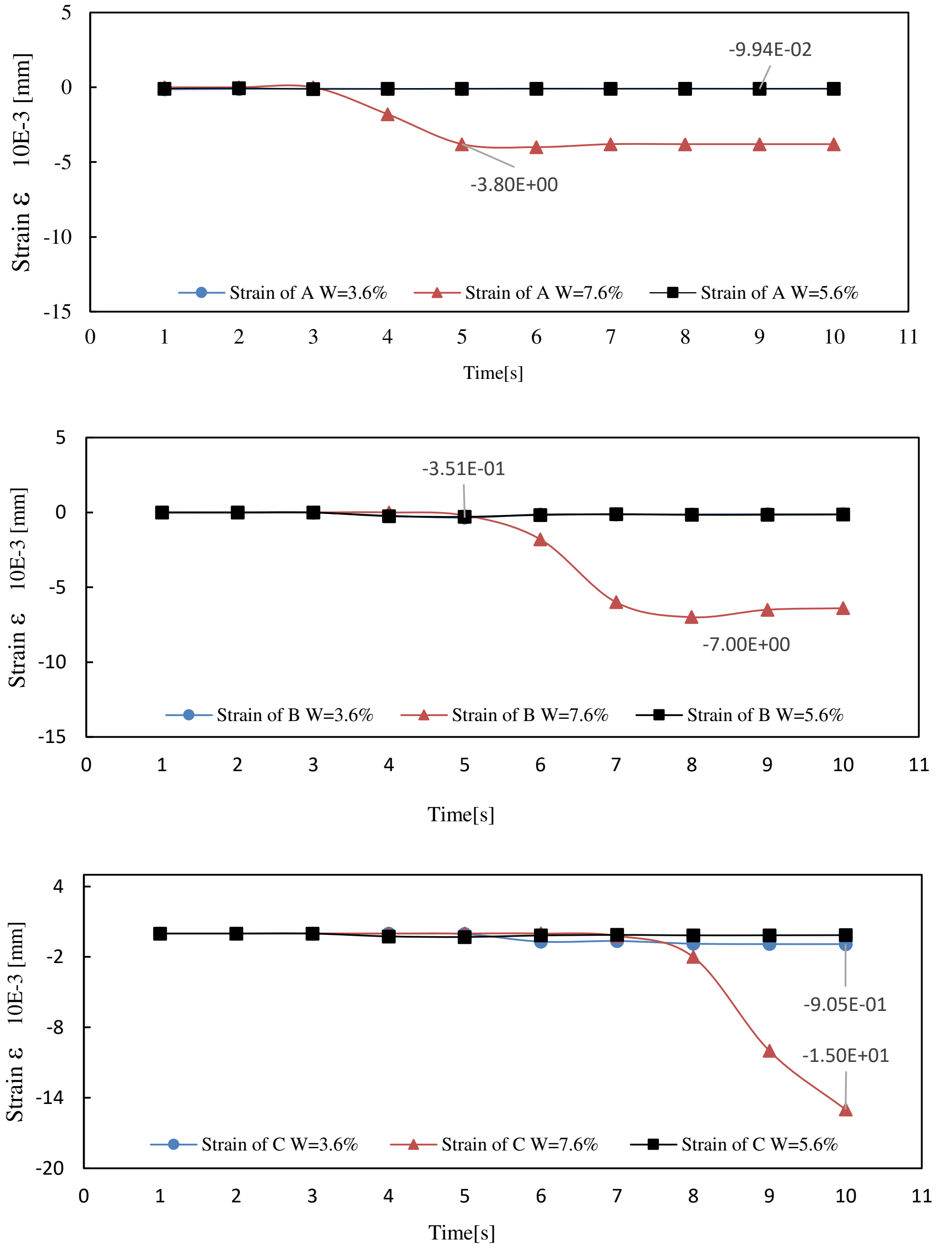

Figure 13. The ballast strain under ω= 3.6%, 5.6%,7.6% in the abutment, backfill and open track

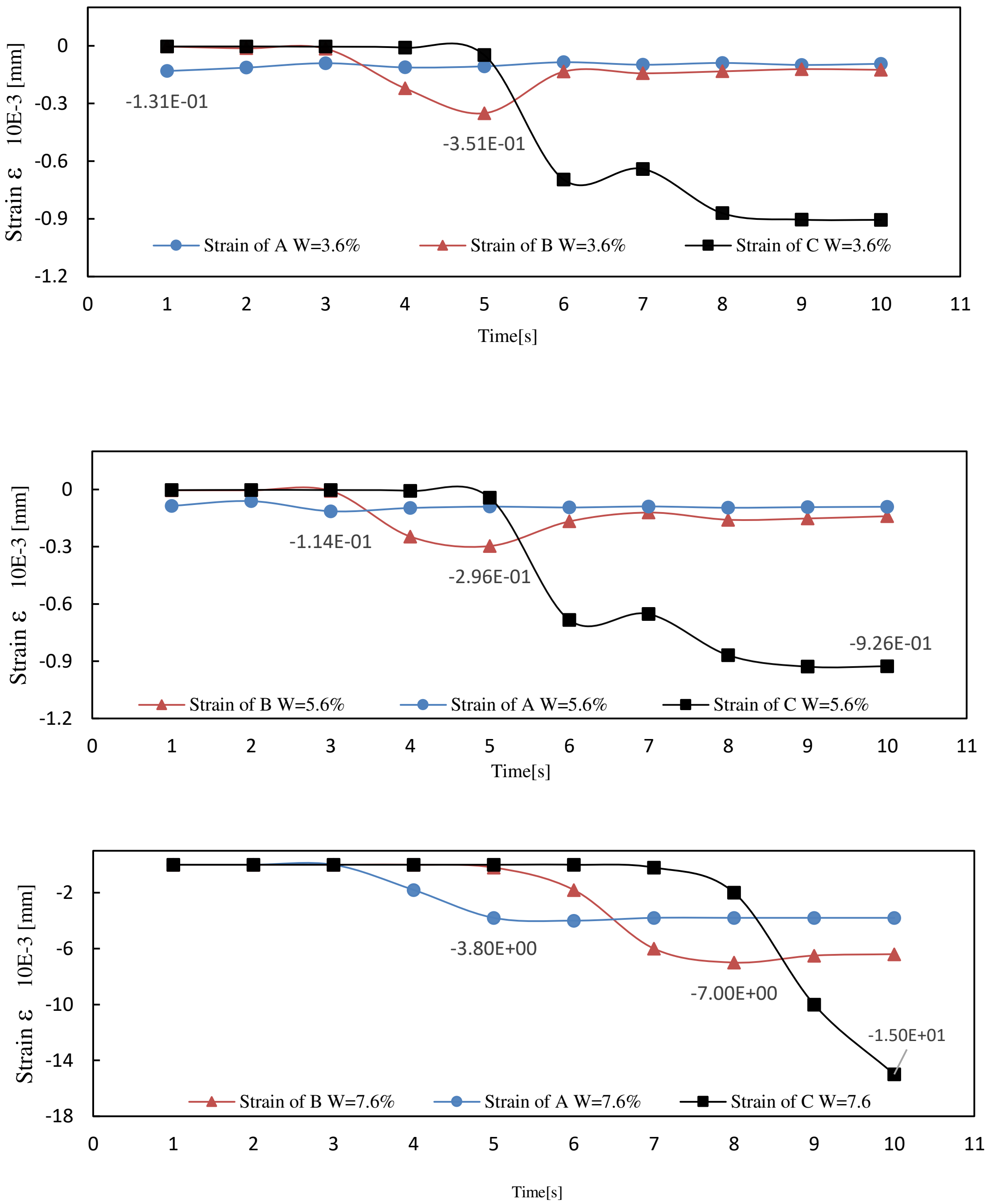

Figure 14. The ballast strain of stress points A, B, C under ω= 3.6%, 5.6%,7.6% separately.

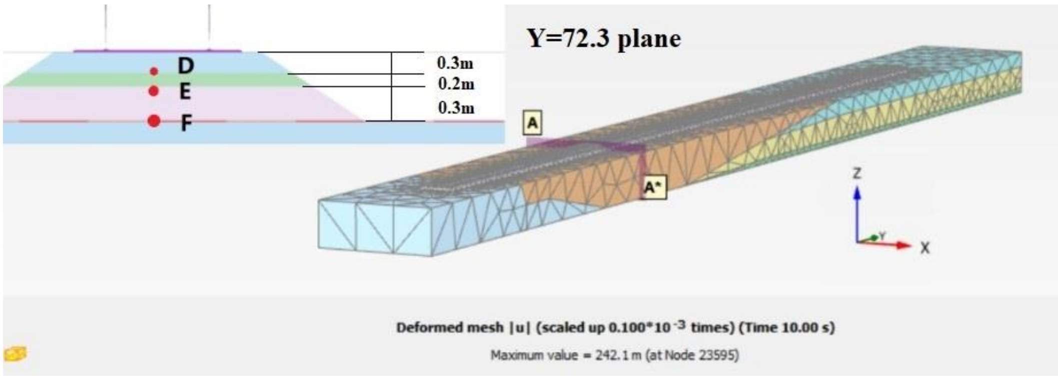

Figure 15. The cross-section A-A* and location of measuring point DEF

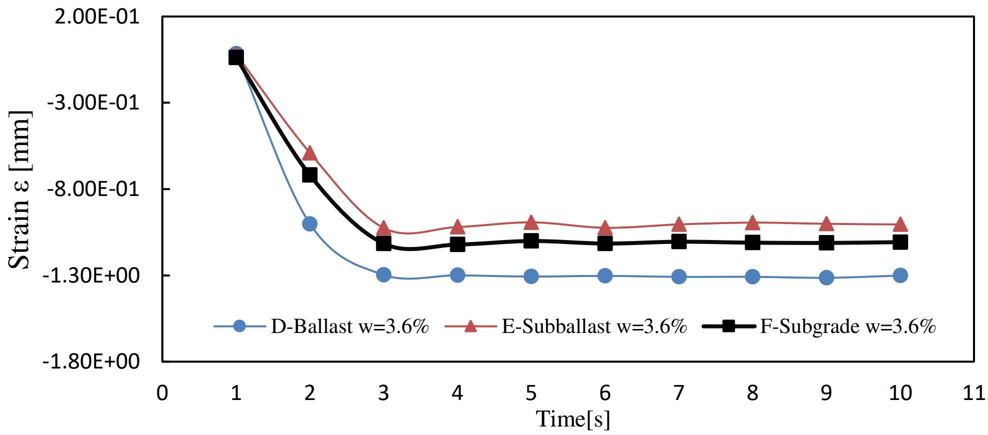

Figure 16 The strain of ballast, subballast and subgrade under ω=3.6%

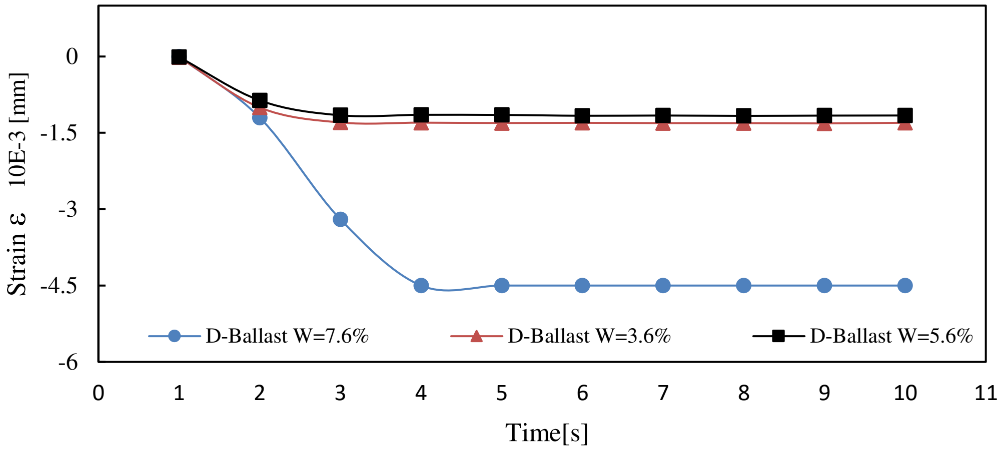

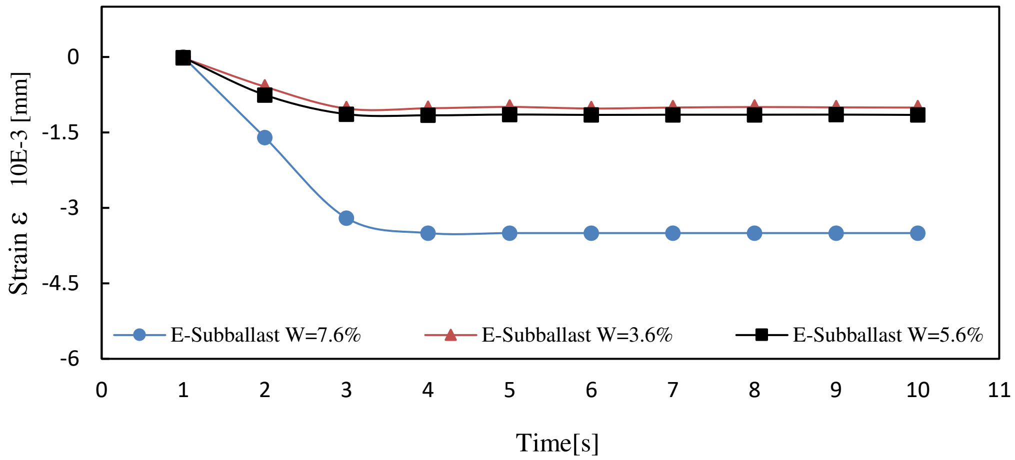

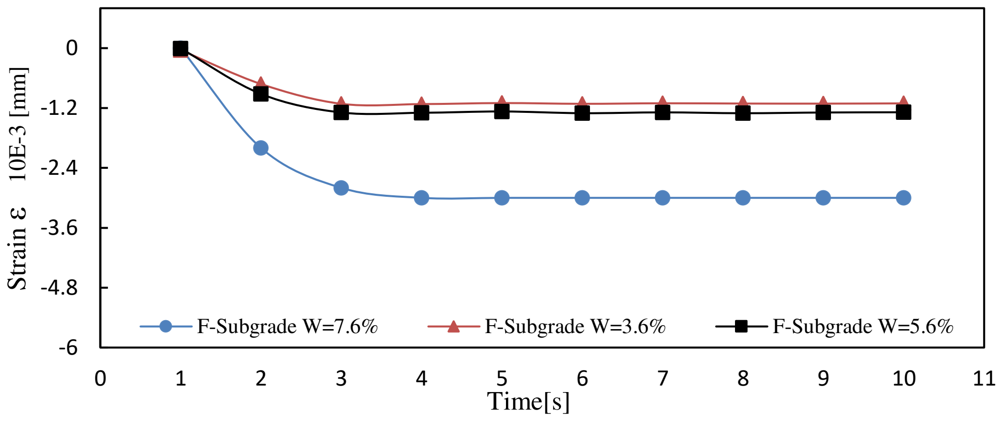

Figure 17 The strain of substructure layers under ω= 3.6%, 5.6%,7.6%.

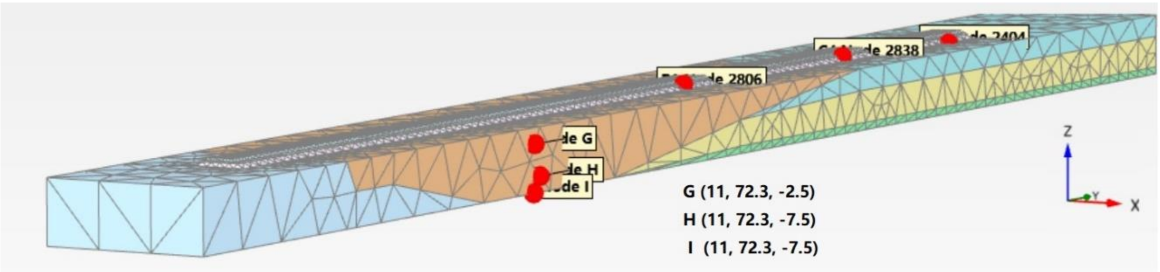

Figure 18 The location of measuring point GHI

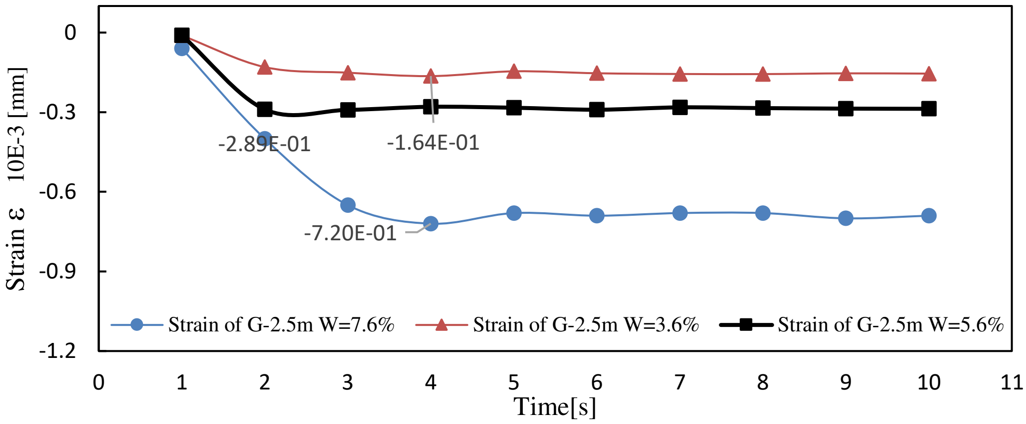

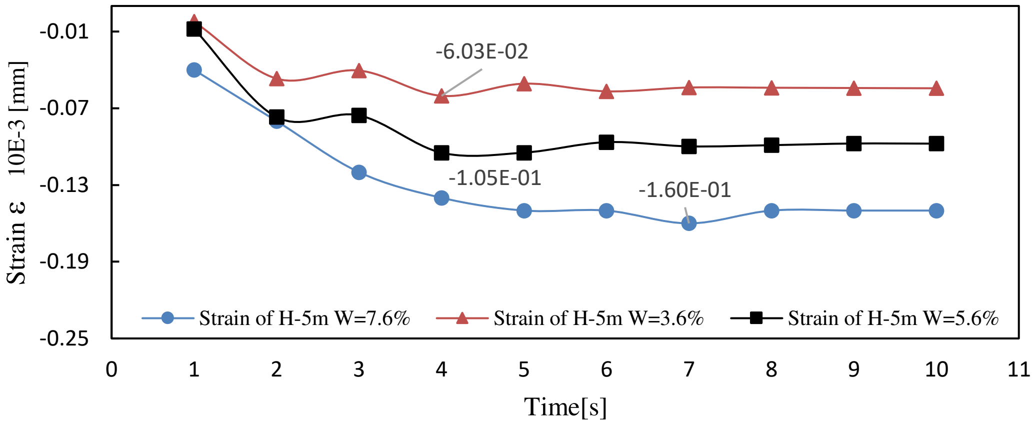

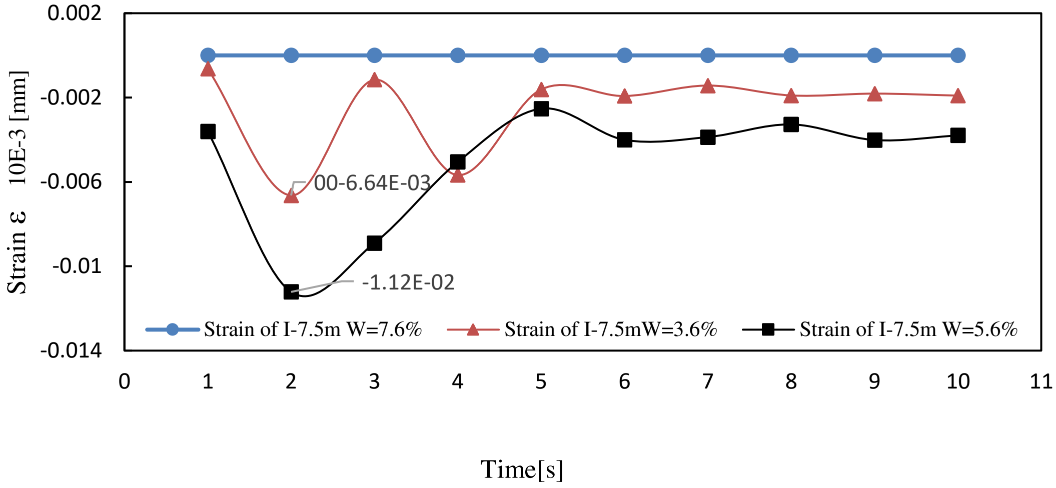

Figure 19 The strain of backfill material varying with depth under ω= 3.6%, 5.6%,7.6%.

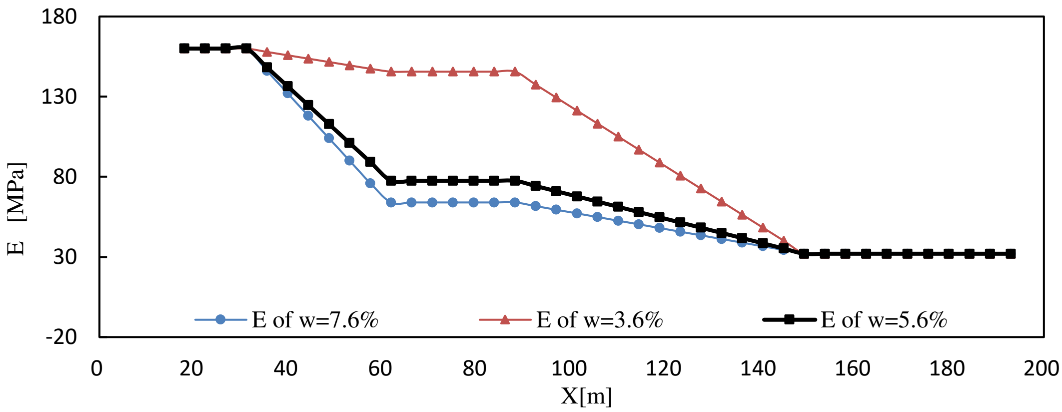

Figure 20The Young's modulus of subsoil under ω= 3.6%, 5.6%,7.6%.

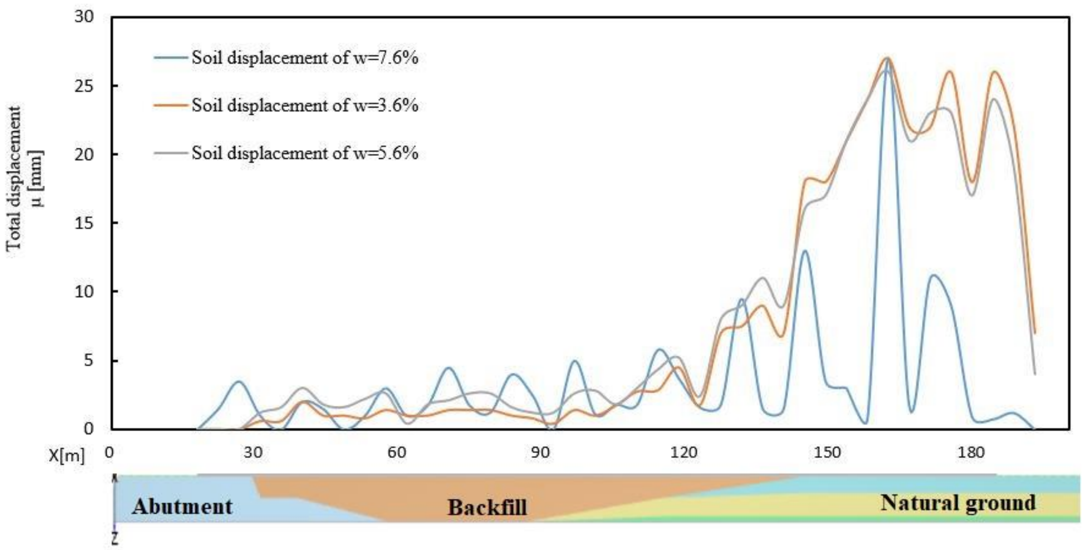

Figure 21 The displacement of the formation along the track under ω= 3.6%, 5.6%,7.6%

List of Tables

Table 1 Material properties of the subsoil......59

Table 2 Material properties of embankment layers......59

Table 3 Material property of sleeper......60

Table 4 Technical details of the simulated train......60

Table 5 Parameters of van Genuchten equation for subsoil (after Tinjum et al., 1997, reproduced with permission)......60

Table 6 Water content of transition subsoils under compaction control (after Paixão et al., 2013, reproduced with permission)......60

Table 7 The resilient modulus of UGM under different water condition calculated from four approaches......61

Table 8 The maximum ballast strain in abutment, backfill, open track section under ω=3.6%,5.6%,7.6%......61

Table 9 The differential settlement under ω= 3.6%, 5.6%,7.6%......61

Table 1.Material properties of the subsoil

Layer type	Thickness (m)	Unit weight (kN/m^3)	Young's modulus (kN/m^2)	Poisson ratio
Abutment	7.5	23	1.60E+05	0.25
Backfill	7.5	20	8.00E+04	0.3
Clay	2.7	20	6.00E+03	0.35
Silt	3.9	13	1.20E+04	0.35
Sand	0.9	20	2.40E+05	0.35

Table 2. Material properties of embankment layers

Embankment layer	Drainage type	Thickness (m)	Unit Weight (kN/m^3)	Young's modulus (kN/m^2)	Poisson ratio	Shear modulus kN/m^2	Oedometer modulus (kN/m^2)	Cohesion (kN/m^2)	Friction angle °
Ballast	Drained	0.3	19	3.00E+05	0.2	1.30E+05	3.17E+05	5	40
Subballast	Undrained A	0.2	22	5.50E+04	0.3	2.20E+04	6.60E+04	10	40
Subgrade	Undrained A	0.3	19.5	4.30E+04	0.3	1.59E+04	6.90E+04	20	28

Table 3. Material property of sleeper

Young's modulus in axial direction (kN/m^2)	Unit Weight (kN/m^3)	Beam cross section area (m^2)	Moment of inertia against bending around the second axis (m^4)	Moment of inertia against bending around the third axis (m^4)
3.60E+07	25	5.13E-02	2.45E-04	2.54E-02

Table 4. Technical details of the simulated train

	Length(m)	Velocity(m/s)	Moving load(kN)	Axles interval (m)	Bogies interval(m)
Train	21.7	20	128	2.7	16.3

Table 5. Parameters of van Genuchten equation for subsoil (after Tinjum et al., 1997, reproduced with permission)

Soil texture	θ_r	θ_S	α	n	M
Coarse	0.025	0.366	0.043	1.521	0.145
Medium	0.010	0.392	0.025	1.169	0.179
Medium fine	0.010	0.412	0.008	1.218	0.079
Fine	0.010	0.481	0.019	1.086	0.068

Table 6. Water content of transition subsoils under compaction control (after Paixão et al., 2013, reproduced with permission)

	Average$\boldsymbol{\omega}$(%)	$\boldsymbol{\omega_{OPM}}$(%)	Median $\boldsymbol{\omega}-\boldsymbol{\omega_{OPM}}$(%)	Number of tests	$\boldsymbol{\rho_{dOPM}}(\boldsymbol{g}/\boldsymbol{cm^3})$

UGM	5.9	5.6	0.4	159	2.23

Table 7. The resilient modulus of UGM under different water condition calculated from four approaches

Water content ω (%)	Resilient modulus M_r (kPa)			
	Huang 1993	Ceratti et al. 2004	Yang et al. 2005	Seed et al. 1962
5.9 (average)	186365	34148	74300	39731
5.6 (OMC)	186365	40809	774609	40584
3.6 (Below OMC)	186434	302254	145586	40016
7.6 (Above OMC)	186296	15633	64014	37500

Table 8. The maximum ballast strain in abutment, backfill, open track section under ω=3.6%, 5.6%, 7.6%

Water content, w	Ballast strain ε (mm)	Abutment ε_A	Backfill ε_B	Open track ε_C
3.6%		-0.10	-0.35	-0.91
5.6%		-0.11	-0.30	-0.93
7.6%		-3.80	-7.00	-15

Table 9. The differential settlement under ω= 3.6%, 5.6%,7.6%

Water content, w	Strain $\varepsilon_B - \varepsilon_A$ (mm)	Strain $\varepsilon_C - \varepsilon_B$ (mm)
3.60%	0.18	0.56
5.60%	0.25	0.63
7.60%	3.20	8.00

APPENDICES

List of Appendices

Appendix A Coordinates of measurement points 63

Appendix B The maximum strain of substructure layers under ω= 3.6%, 5.6%,7.6% 64

Appendix C The maximum strain of backfill with the depth of 2.5m, 5m, and 7.5m under ω= 3.6%, 5.6%,7.6% 65

Appendix D The soil deformation at formation when t=6s in case of the water content 3.6%, 5.6%, 7.6%. 66

Appendix A Coordinates of measurement points

Point	X	Y	Z
A, B, C are on the surface of ballast in abutment, backfill, embankment section			
Point A	11	23.8	1
Point B	11	72.3	1
Point C	11	168.4	1
D, E, F are on the surface of subballast, subgrade and formation in the backfill section			
Point D	11	72.3	0.7
Point E	11	72.3	0.5
Point F	11	72.3	0
G, H, I are in depth of -2.5m, -5m, -7.5m in the backfill section			
Point G	11	72.3	-2.5
Point H	11	72.3	-5
Point I	11	72.3	-7.5

Appendix B The maximum strain of substructure layers under ω= 3.6%, 5.6%,7.6%

Water content ω (%)	Ballast ε_D (mm)	Subballast ε_E(mm)	Subgrade ε_F(mm)
3.6	-1.30	-1.03	-1.12
5.6	0.00	0.00	0.00
7.6	-4.50	-3.50	-3.00

Appendix C The maximum strain of backfill with the depth of 2.5m, 5m, and 7.5m under ω= 3.6%, 5.6%,7.6%

Water content ω (%)	Backfill strain ε (mm)	G(-2.5)	H(-5)	I(-7.5)
3.6		-0.16	-0.06	-0.01
5.6		-0.29	-0.10	-0.01
7.6		-0.72	-0.16	0.00

Appendix D The soil deformation at formation when t=6s at location of X=120 in case of the water content 3.6%, 5.6%, 7.6%.

The soil deformation when t=6s, at location of X=120 under water content is 3.6%

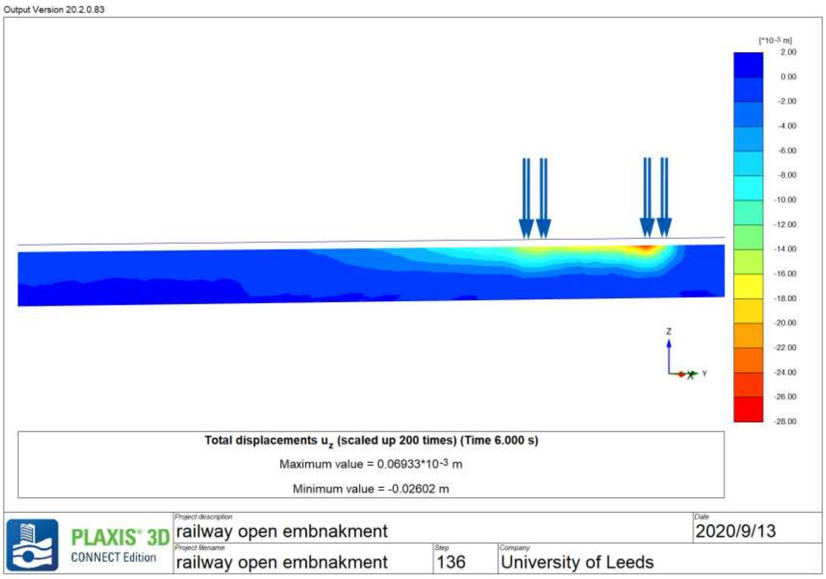

The soil deformation when t=6s at location of X=120 under water content is 5.6%

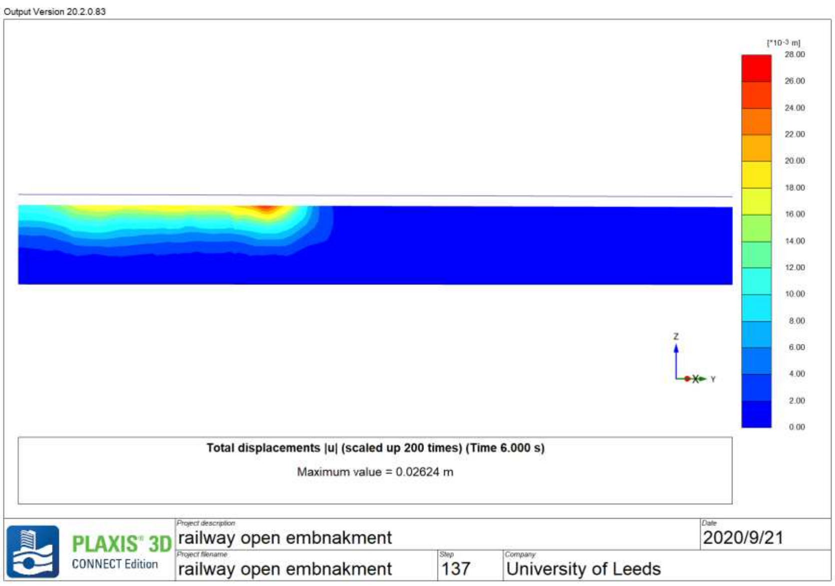

The soil deformation when t=6s at location of X=120 under water content is 7.6%